Journal of Asian Earth Sciences 218 (2021) 104875

Contents lists available at ScienceDirect

Journal of Asian Earth Sciences

journal homepage: www.elsevier.com/locate/jseaes

Application of chemometrics to quantitative source assessment of crude oils from the Zhanhua Depression, Bohai Bay Basin, northeast China

Xiao–Hui Lin [a,b], Zhao–Wen Zhan [a], Yan–Rong Zou [a,*], Tian Liang [a,b], Ping'an Peng [a]

[a] State Key Laboratory of Organic Geochemistry, Guangzhou Institute of Geochemistry, Chinese Academy of Sciences, Guangzhou 510640, China
[b] University of Chinese Academy of Sciences, Beijing 10039, China

ARTICLE INFO

Keywords:
The Zhanhua Depression
Chemometrics
Biomarkers
Oil–oil correlation

ABSTRACT

The chemometric methods alternating least squares and multidimensional scaling were employed in this study to quantify the relative contribution of the sources and identify the affinities of sixty–five crude oil samples collected in the Zhanhua Depression. The circos diagram was used to reflect the relative contributions of different source rocks. Based on these techniques, two end–members (EMs) were identified which represent the geochemical characteristics of two regional source–rocks (Es_3^L and Es_4^U). The EM1 composition assigned to Es_3^L is characterized by relatively low C_{35}/C_{34} homohopane ratio and relatively low abundance of gammacerane. This EM is consistent with a source facies that was deposited in freshwater lacustrine environment that contained a non–stratified water column and suboxic to dysoxic bottom waters. Distributions of the regular steranes and tricyclic terpanes, the relatively low steranes/hopanes ratio suggest the organic matter input into this source facies were combined microalgal material and terrestrial organic matter. Oils from the Bonan Sag and Gubei Sag were derived mainly from this source facies. In contrast, EM2 has been assigned to the Es_4^U source rock and is characterized by relatively high abundance of gammacerane, C_{35}/C_{34} homohopane ratio greater than one, suggesting deposited in a saline to hypersaline lacustrine environment that contained a stratified water column with strongly reducing bottom waters. Distributions of the regular steranes and tricyclic terpanes as well as relatively high steranes/hopanes ratio suggest the organic matter deposited in this setting was mainly derived from microalgal/bacterial sources. Oils from the Luojia Nose and Chanjiazhang High were derived mainly from this source facies. Mixed contributions of these two source facies (end–members) account for the compositions of crudes produced in the Yihazhuang Arch and Gudao High. In the case of the Yihezhuang Arch the crudes appear to have near equal contributions from the two source faces, whereas crudes from the Gudao High appear to have slightly higher contributions from the Es_3^L source facies than from the Es_4^U source facies.

1. Introduction

The Bohai Bay Basin is one of the most petroliferous basins in China (Hao et al., 2010). The Jiyang Superdepression in the southeast of the Bohai Bay Basin (Fig. 1a) covers an area of 25510 km^2 (Wang et al., 2015) and consists of four depressions from south to north, that is the Zhanhua, Dongying, Huimin, and Chenzhen depressions, and many secondary structural units (Zhang et al., 2011). The Zhanhua Depression located in the east of the Jiyang Superdepression is a faulted lacustrine depression developed under the background of Palaeozoic structural activities (Shi et al., 2005). The hydrocarbon accumulation and reservoirs formation in the Zhanhua Depression has a close relationship with fault activity (Wang et al., 2015; Sun et al., 2015; Shi et al., 2005). The petroleum in different reservoirs show different geochemistry characteristics due to the mixture during or after hydrocarbon accumulation.

Although several studies were carried out on the Zhanhua Depression, the geochemical characteristics of the crude oils are not understood. It is known that the oil and gas in most reservoirs are derived from deep source rocks (Xie et al., 2006) and the hydrocarbon subsequently migrated up through fault–fracture mesh networks to different sags (Wang et al., 2005). But the relative contributions of different source rocks have not been identified. Chemometric methods have unique advantages with respect to the comprehensive consideration of the effects of multiple parameters, genetic classification and correlation of mix oils (Peters et al., 2007; Peters et al., 2008a). The statistical algorithms employed during chemometric analysis provide a more quantitative

* Corresponding author.
E-mail address: zouyr@gig.ac.cn (Y. Zou).

https://doi.org/10.1016/j.jseaes.2021.104875
Received 30 June 2020; Received in revised form 16 June 2021; Accepted 27 June 2021
Available online 1 July 2021

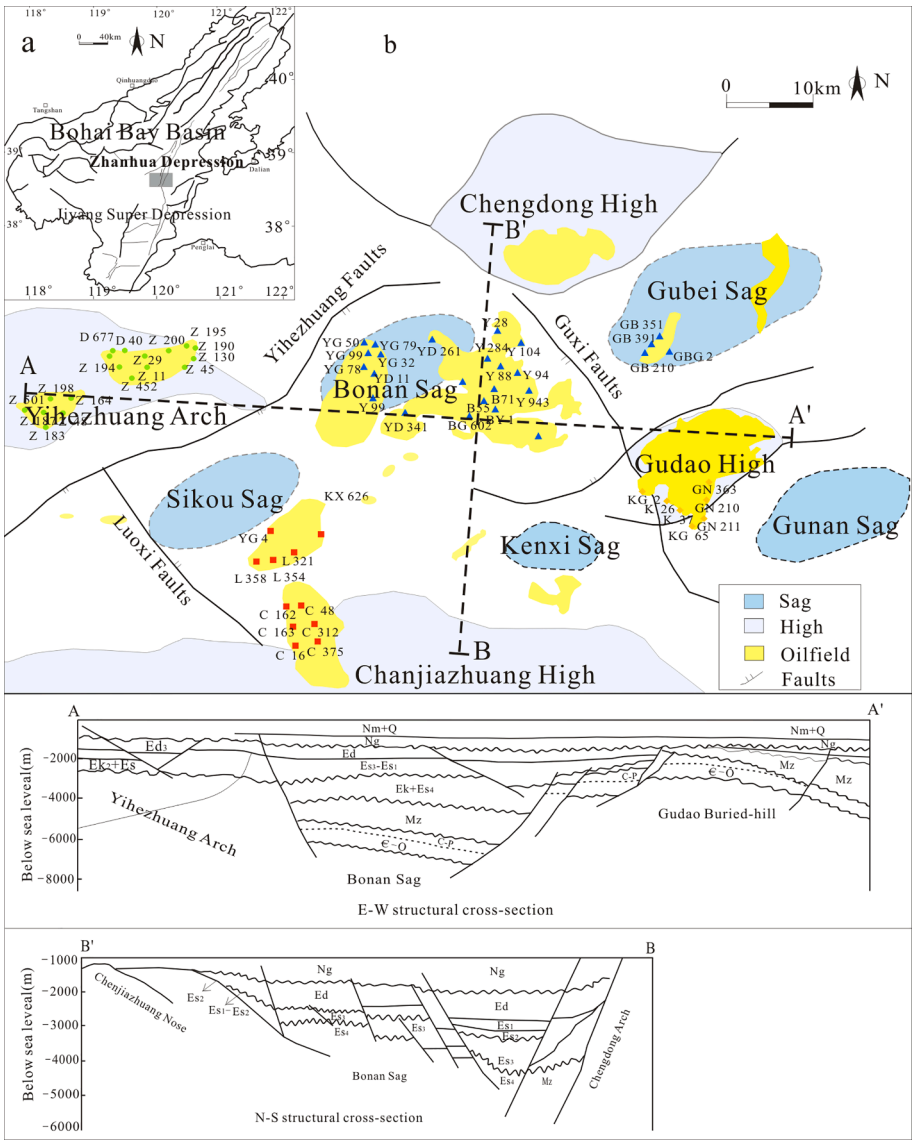

Fig. 1. Study area and sample locations. (a) Location of the study area in the Bohai Bay Basin, China (Yu et al., 2020), (b) structural features and distribution of crude oil samples in the Zhanhua Depression (Zhang et al., 2015), and structural cross sections (A–A′ and B–B′).

estimation of the contribution of source rocks for the mixed oils than that obtained through traditional qualitative geochemical methodologies. In this study, we have applied chemometric methods to organic geochemical parameters from a suite of crude oils collected in the Zhanhua Depression. Alternating least squares (ALS, Peters et al., 2008b; Zhan et al., 2016a) was employed to determine the sources of oils and multidimensional scaling (MDS, Wang et al., 2016) was used for oil–oil correlation. The visualization tool, circos, was used to reveal the relationships between endmembers and oils.

2. Geological setting

The Jiyang Superdepression is bounded by various structures (Huang and Liu, 2014): Tan–Lu Fault to the east, arcuate Chengning Uplift to the west and north, and Qi–Guang Fault to the south (Zhang et al., 2012). The geologic framework of the Jiyang Superdepression is complex due to the counter–inclined block faulting, basin–inclined fault depression, and monolithic depression that occurred from the Paleogene to Neogene (Li et al., 2004). The Zhanhua Depression lies at the northeast of the Jiyang Superdepression (Lu et al., 2012; Fig. 1a) has experienced multi–period tectonic movements, such as the Indosinian, Yanshan, and Himalayan movements (Lin et al., 2007). Due to strong tectonic activities, petroleum generated in deeply buried source rocks migrated to shallower reservoirs. The tectonic units within the Zhanhua Depression include the Bonan Sag in the center, Gubei Sag in the northeast, Yihezhuang Arch in the west, Luojia Nose and Chenjiazhuang High in the south, Gudao High in the east, and Chengdong High in the north (Fang, 2017; Fig. 1b). The depositional centre of the Zhanhua Depression includes the Bonan Sag and Gubei Sag (Zhang et al., 2007). The hydrocarbon accumulation stratigraphy of the Zhanhua Depression comprises the Paleogene Kongdian (Ek), Shahejie (Es), and Dongying (Ed) formations, Neogene Guantao (Ng) and Minhuazhen (Mz) formations (Hao et al., 2009; Fig. 1). The oil and gas reservoirs in the Zhanhua Depression are mostly related to the Neogene reservoirs. The lower third and upper fourth members of the Shahejie Formation (Es_3^L and Es_4^U) are considered as the major hydrocarbon source rocks (Li et al., 2010). Late–stage faulting activities occurred in the end of the Neogene and cut through the Es_3 and Es_4 source rocks in the Bonan Sag and Gubei Sag (Li et al., 2010), which provided good migration channels for oil and gas migration.

The source rocks were buried at the depth of 3000 m to 5000 m (Zhang et al., 2011). The Es_4^U member is mainly composed of lime–shale,

Table 1
Basic information of the samples and geochemical parameters discussed in this study.

Location	Well	Member	Depth/m	PM. B	$\delta^{13}C_{Oil}$ /‰	δ^{13}Csat. /‰	$\delta^{13}C_{Aro.}$ /‰	Pr/ Ph	Pr/ n–C_{17}	Ph/ n–C_{18}	$\sum nC_{21-}/\sum nC_{22+}$	25 N–$C_{29}H$/ $C_{30}H$
Bonan–Gubei Sag	Y28	Es_3	3461	0	−26.8	−27.4	−26.2	1.08	0.38	0.39	1.39	0.03
	Y123	Es_3	3733–4666	0	−26.4	−27.2	−25.8	1.47	0.41	0.29	1.35	0.03
	Y943	Es_3	3155–3163	0	−26.6	−27.3	−25.9	1.62	0.3	0.2	1.81	0.03
	YD261	Es_2	3304–3383	0	−26.9	−27.7	−25.9	1.92	3.14	0.5	0.81	0.04
	Y94	Es_4	3505–3520	0	−25.6	−26.3	−24.9	0.94	0.31	0.35	1.56	0.03
	Y284	Es_3	3901–4130	0	−26.1	−26.6	−25.1	1.23	0.36	0.33	1.86	0.03
	Y104	Es_3	4011–4030	4	−26.1	−26.5	−25.2	–	–	–	–	0.04
	Y170	Es_4	3806–3829	0	−26.3	−26.9	−25.6	0.75	0.35	0.51	2.27	0.06
	YG78	O	1838–1848	0	−25.9	−26.8	−24.9	1.13	0.5	0.44	0.99	0.04
	YG50	O	1957–1970	0	−26.1	−26.8	−25.3	1.08	0.38	0.38	1.18	0.04
	YG32	Mz	2639–2643	0	−26.0	−26.9	−25.4	1.1	0.37	0.35	1.43	0.04
	YG99	O	2044–2126	0	−25.9	−26.7	−25.4	1.01	0.37	0.4	1.49	0.04
	YD11	O	2150–2168	0	−25.6	−26.3	−25.3	0.96	0.31	0.34	1.39	0.04
	Y71	Es_3	3026–3050	0	−26.4	−27.5	−25.9	1.08	0.41	0.4	1.12	0.05
	Y85	Es_3	3223–3450	0	−26.2	−27.0	−25.6	1.37	0.38	0.29	1.45	0.04
	Y99	Ek	3450–3500	0	−26.4	−27.5	−26.2	0.94	0.38	0.41	1.23	0.04
	Y171	Es_4	3775–3880	0	−26.3	−27.0	−25.5	0.83	0.27	0.36	1.78	0.06
	YD341	Es_4	3676–3790	0	−25.6	−25.9	−24.6	0.73	0.26	0.39	2.11	0.05
	YG79	O	1904–2025	0	−24.8	−25.7	−24.2	0.79	0.31	0.43	1.13	0.04
	Y88	Es_3	2994–3001	0	−26.7	−27.4	−26.1	1.06	0.49	0.48	1.21	0.04
	Y50	Es_1	3070–3180	0	−26.5	−27.2	−25.7	1.17	0.4	0.34	1.73	0.04
	B71	Ng	1500	3	−26.4	−28.3	−25.9	0.83	–	–	–	0.04
	BY1	Es_3	3605–3628	0	−25.7	−27.0	−25.6	0.81	0.38	0.53	1.2	0.05
	B55	Ng	1301–1350	1	−26.4	−28.4	−25.8	0.7	0.57	0.96	0.62	0.05
	BG602	Ed	2811–2814	0	−28.5	−29.3	−28.0	1.17	0.78	0.69	0.91	0.10
	GBG2	C-P	3580–3583	4	−26.1	−26.9	−25.2	–	–	–	–	0.04
	GB210	Es_3	2838–2844	0	−26.4	−26.7	−26.1	1.56	0.54	0.38	1.3	0.06
	GB351	Es_3	2967–2980	0	−25.6	−26.3	−25.0	1.44	0.37	0.28	1.54	0.04
	GB391	Es_3	2967–2976	0	−25.7	−26.6	−25.1	1.45	0.37	0.28	1.75	0.04
Yihezhuang Arch	Z130	Ed	1380–1389	3	−28.4	−27.8	−25.3	0.51	1.15	2.42	1.24	0.04
	Z183	Ng	1182–1187	3	−24.3	−28.3	−25.6	–	–	–	–	0.05
	Z194	Ng	1324–1332	0	−25.6	−27.8	−25.6	0.67	0.68	1.09	5.66	0.04
	Z164	Ng	1226–1229	3	−25.4	−28.3	−25.7	–	–	–	–	0.04
	Z190	Ng	1300–1301	3	−25.5	−28.2	−25.6	0.95	3.67	2.18	0.47	0.04
	Z501	Ng	1128–1132	2	−26.3	−28.3	−25.7	1.31	0.39	0.27	0.48	0.04
	Z187	Ng	1174–1178	3	−26.3	−28.4	−25.6	–	–	–	–	0.04
	Z48	Ng	1297–1311	3	−26.1	−28.2	−25.4	–	–	–	–	0.04
	Z452	Ng	1285–1289	3	−26.6	−28.7	−25.8	–	–	–	–	0.04
	Z198	Mz	1336	3	−26.3	−28.6	−25.8	0.85	0.63	0.76	0.27	0.05
	Z45	Ed	1319–1321	3	−26.5	−28.4	−25.7	–	–	–	–	0.05
	Z29	Ng	1152–1158	3	−26.5	−28.3	−25.6	1.21	0.98	1.29	1.06	0.04
	Z195	Ed	1401–1411	2	−26.4	−29.2	−26.3	0.83	0.81	1.04	3.74	0.04
	Z9	Ng	1430–1500	3	−26.2	−28.1	−25.2	0.91	–	–	–	0.05
	Z11	Ng	1421–1440	2	−26.1	−27.5	−25.6	0.96	0.93	1	0.88	0.04
	Z200	Ng	1339–1348	3	−26.1	−28.3	−25.7	–	–	–	–	0.04
	D40	Es_4	2853–2866	0	−26.9	−27.4	−26.5	0.86	0.47	0.54	1.36	0.04
	D677	C-P	2870–2886	1	−27.2	−27.9	−26.9	1.22	0.6	0.57	0.81	0.06
Gudao High	KG2	Mz	2827–2852	0	−26.9	−25.9	−24.5	1.67	0.57	0.41	1.37	0.05
	K37	Es_2	2114–2150	0	−25.2	−25.9	−24.6	2.23	0.41	0.2	1.18	0.05
	KG65	Ed	1554–1583	3	−26.5	−28.3	−25.6	0.28	0.36	2.63	0.88	0.04
	K26	Es_4	2900–2933	0	−25.6	−27.0	−25.3	0.76	0.3	0.4	1.07	0.13
	GN210	Ek	1346–1349	3	−26.5	−28.6	−25.8	–	–	–	–	0.02
	GN211	Ek	1347–1349	3	−26.2	−27.8	−25.6	0.33	0.71	1	0.27	0.04
	GN363	Es_2	2637–2640	0	−27.0	−27.6	−26.4	1.22	0.53	0.45	1.36	0.05
Luojia–Chenjiazhuang High	KX626	Es_4	2634–2647	0	−26.4	−27.2	−26.2	0.54	0.32	0.56	1.4	0.05
	YG4	Mz-Pz	1466–1600	3	−26.0	−27.9	−25.5	–	–	–	–	0.04
	L354	Es_3	2654–2657	0	−27.3	−26.6	−25.4	0.52	0.33	0.62	0.86	0.04
	L358	Es_4	2663–2691	0	−26.2	−28.2	−27.3	0.42	0.64	1.41	1.1	0.03
	L321	Es_3	1793–1800	0	−26.5	−26.9	−26.5	0.54	0.36	0.69	1.18	0.04
	C312	Es_3	1321–1364	3	−26.2	−28.6	−25.8	–	–	–	–	0.05
	C48	Ng	1335–1337	2	−26.3	−28.9	−26.0	1.03	–	–	–	0.05
	C375	Ng	1253–1258	3	−26.3	−28.7	−25.8	–	–	–	–	0.05
	C163	Ed	1457–1463	3	−26.2	−28.1	−25.9	0.47	–	–	–	0.05
	C16	Ng	1247–1253	3	−26.2	−28.6	−25.9	–	–	–	–	0.05
	C162	Es_3	1800–1806	2	−26.8	−28.3	−26.8	0.36	0.53	1.38	0.54	0.04

Note: PMB: degree of biodegradation by Peters and Moldowan (1993). $\delta^{13}C_{Oil}$ /‰, δ^{13}Csat. /‰ and $\delta^{13}C_{Aro.}$ /‰ are the stable carbon isotope ratios (/‰) for whole oil, saturate and aromatic fractions, respectively. 25 N-$C_{29}H/C_{30}H$ = C_{29}–norhopanes/C_{30} hopane.

dolomite–mudstone, and dark mudstone (Wang et al., 2017). These rocks typically contain 1.5%–4.0% TOC, with predominantly mixed type I/II kerogens, and the hydrogen indices range from 306 to 467 mg/g (Wang and Hu, 2014). During the deposition of the Es_4 member, the block faulting activities were intensive and the basin was separated into many independent blocks (Fang, 2017). This promoted the formation of hydrologically isolated lake basins where evaporation of the lake waters led to the development of saline lacustrine facies. The Es_4 shale was deposited in saline–hypersaline lacustrine environments with variable water depths (Wang et al., 2005). The upper Es_4 member in large parts of the Bonan Sag and Gubei Sag is currently thermally mature, the deepest portions are beyond peak oil generation (Chen et al., 2011; Zhang et al., 2004). The Es_3 member is generally composed of massive dark mudstone, contains more than 3% TOC and type I kerogen with the hydrogen indices ranging from 261 to 516 mg/g. The Es_3 member was deposited during the formation process of deep lake basin. The Es_3^L shale was deposited in freshwater to brackish and semi–deep to deep lacustrine environments (Jiu et al., 2013; Shi et al., 2005).

3. Samples and methods

3.1. Samples

Sixty–five crude oil samples were collected from the Zhanhua Depression, Bohai Bay Basin, China. They were recovered from different depths and reservoirs. In total, 29, 18, 7, and 11 crude oil samples were collected from the Bonan–Gubei Sag, Yihezhuang Arch, Gudao High, and Luojia–Chenjiazhuang High, respectively. The sample locations are shown in Fig. 1b. The basic information of the oil samples, including reservoir layer, depth, and level of biodegradation, is presented in Table 1.

3.2. Analytical methods

3.2.1. GC analysis of the whole oils

The whole oils were analysed with a Shimadzu 2010Plus gas chromatograph (GC) equipped with an FID and HP–5MS capillary column (50 m × 0.32 mm i.d., 0.52 μm film thickness). A measured volume of *n*–hexane was added to each ~ 10 mg oil sample. The oven temperature was initially held at 35 °C for 2 min, then programmed to reach 295 °C at a rate of 3 °C/min, and then held at 295 °C for 30 min. The temperature of the injector was 290 °C. The carrier gas is Helium and the flow rate is 1.0 mL/min.

3.2.2. Oil fractions

Asphaltenes were separated from the crude oils by centrifugal precipitation with *n*–hexane. The supernatant portion was subsequently separated into saturates, aromatics, and resins by column chromatography, using mobile phases of *n*–hexane, *n*–hexane/dichloromethane (DCM; 2:1 v/v), and DCM/methanol (1:1 v/v), respectively, and a stationary phase of silica and alumina (2:1 v/v).

3.2.3. Carbon isotope of the whole-oil and oil fractions

A Finnigan Delta^{plus} XL IRMS instrument coupled to a CE flash 1112 EA via a Conflo III interface was used to measure the stable carbon isotope compositions of the whole oils and their saturated and aromatic fractionations. The CO_2 reference gas was calibrated using the NBS–22 oil standard, and a working standard (black carbon) was measured to monitor the system. The temperatures for reduction and oxidation were set to 650 °C and 950 °C, respectively. The stable carbon isotope values are reported relative to VPDB. Each sample was measured at least twice until the error was ≤0.5‰. The final stable carbon isotope results represent the averages of multiple runs.

3.2.4. GC–MS analysis

The GC–MS analyses of saturated hydrocarbons were performed with a Shimadzu QP2010 Ultra GC–MS. The GC separation was completed with a 30 m HP–5MS capillary column (0.25 mm i.d., 0.25 μm film thickness) and the temperature was programmed to reach 140 °C from 50 °C (held for 2 min) at 10 °C/min and finally 300 °C at 2 °C/min (held for 15 min). Helium was used as the carrier gas. The MS was operated in electron ionization mode at a voltage of 70 eV and ion source temperature of 230 °C. The analysis was carried out using mode–combining selective ion monitoring (SIM) with full–scan detection; the scan varies from 50 to 550 Da. The selected ions included *m/z* 191, 217, 218, and 177.

3.3. Chemometric analysis

ALS can be used to deconvolute the mixed crude oil samples, determine the fractional contributions of EMs, and directly calculate the compositions of EM without requiring EM samples (Peters et al., 2008a; Zhan et al., 2016a). The ALS deconvolution based on Pirouette® software (Infometrix, Inc.) was set as range scale preprocessing, which means the biomarker data were first normalised using the maximum–minimum range, that is, $X' = (X - X_{min})/(X_{max} - X_{min})$, thereby giving each individual biomarker ratio equal weight (Wang et al., 2016). The MDS is an effective nonlinear multivariate oil–oil and oil–source correlation tool, which simplifies the multidimensional data volume into a low–dimensional space and identifies an appropriate spatial position by iteration (Wang et al., 2016). The MDS reveals the similarity or dissimilarity between the crude oils based on their spatial positions. Circos is a mature software package created by Zytkow and Rauch (1999). It is an effective visualization tool that is generally used for analysing the similarities and differences of genomes (Martin et al., 2009). In this paper, we employed the circular diagrams of circos to reflect the relative contributions of the EMs. More importantly, it can estimate the volumetric charge of a given source rock to each of the geographic area.

In order to more accurately evaluate the contributions of multiple source facies for the oils by chemometrics, crude oils that had experienced severe biodegradation were removed. We also excluded values of ratios that had very small values because of the associated analytical uncertainty they represent. In this study, 19 source– and depositional environment–related parameters, that is, $C_{19}/C_{23}TT$; $C_{22}/C_{21}TT$; $C_{24}/C_{23}TT$; $C_{24}Te/C_{26}TT$; ETR [ETR=($C_{28}TT + C_{29}TT$)/($C_{28}TT + C_{29}TT$ + Ts)]; $C_{29}H/C_{30}H$; $C_{35}H/C_{34}H$; $C_{31}HR/C_{30}H$; Ga/$C_{30}H$; TT/H; S/H (steranes/hopanes); $C_{29}Ts/C_{29}H$; $C_{30}M/C_{30}H$; C_{27}%, C_{28}%, and C_{29}% ααα steranes as well as stable carbon isotope ratios of the whole oil, saturates, and aromatics, were used in ALS and MDS

3.4. Repeatability and accuracy

Repeatability of oil fractionation, GC and GC–MS analyses was tested by comparing the weight of each group composition and the biomarker ratios for the oils come from close well and some samples were treated twice. Many oil samples from different intervals in a given well are also remarkably similar due to they have undergone similar mixing histories (Peters et al., 2008a). For oils coming from close wells or the same well, the relative contents of each group composition and the biomarker ratios have minor change. If the deviation is comparatively large, the sample would be re–treated once or twice. All samples were treated under the same experiment condition.

Zhan et al (2016b) have proved the reliability of ALS by mixing the three original oils that can be easily differentiated based on their compound compositions and distributions of biomarkers in different proportions, and then calculate the relative contributions and the biomarker parameters of each end–members for the mixed oils by ALS. They found that the computed results were identical to the original oils, the calculation error was less than 6.9%. Lin (2021) has proved the calculation error was less than 10% when the ratios of the biomarkers were used in ALS for unmixing binary mixture. Accuracy of

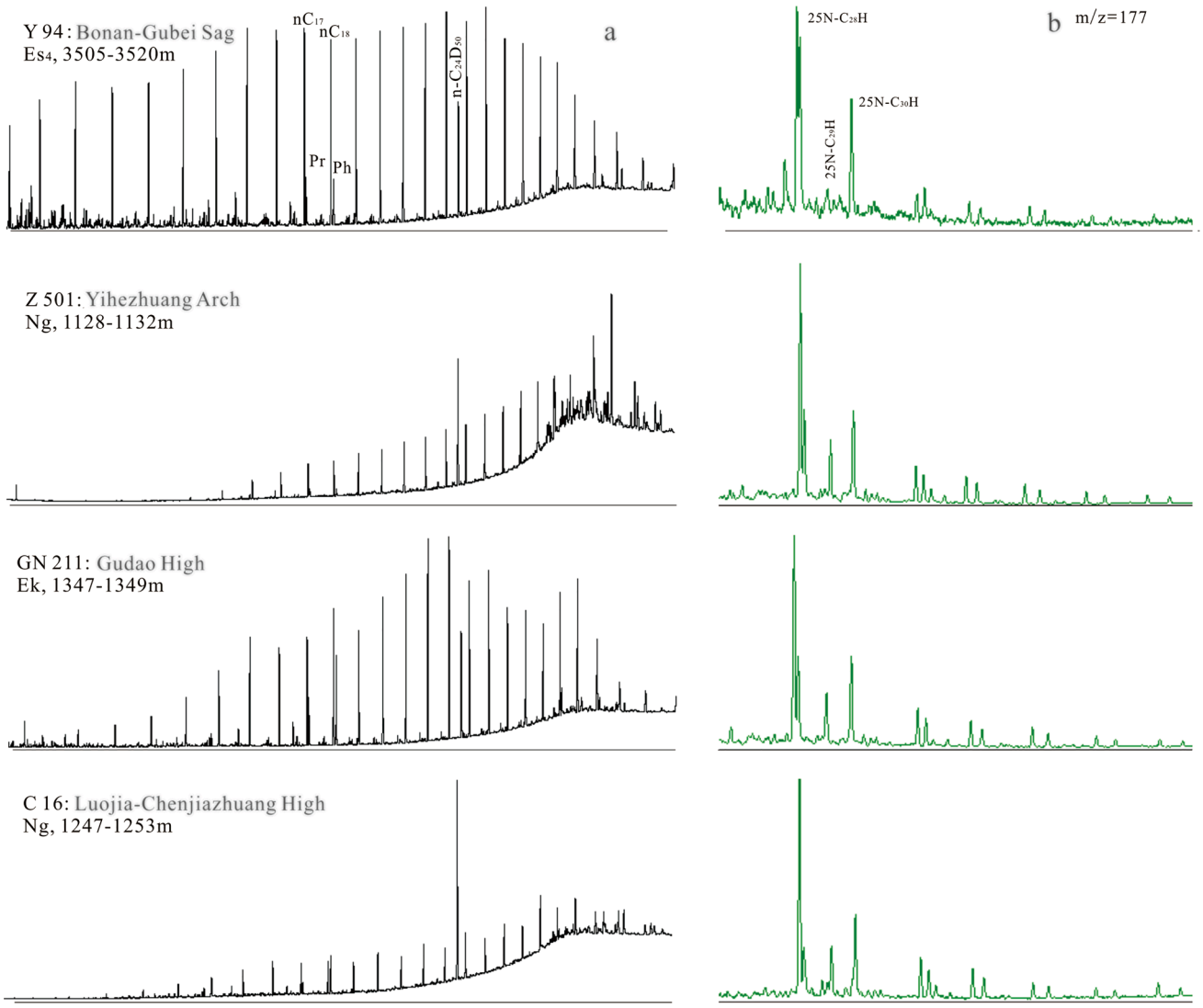

Fig. 2. Representative gas chromatograms of whole oil (GC) showing the distributions of paraffins (a), *m/z* 177 mass chromatograms showing 25–norhopane (N–H) distributions (b). Note: Pr: pristane, Ph: phytane, IS: internal standard (*n*-$C_{24}D_{50}$);25 N-C_{28}H:17α(H),21β(H)–25,30–Bisnorphopane; 25 N-C_{30}H:17α(H),21β(H)–25–Norhopane.

chemometric analyses in this study was also examined by comparing the geochemical characteristics of the end–members obtained by ALS to the source rocks (data collected from previous research). And the contribution of each end–members for different tectonic regions were compared with previous research.

4. Results and discussion

4.1. Stable carbon isotope composition

The stable carbon isotopes of the oils are mostly depending on the organic matter input and depositional environment of the source rocks (Sun et al., 2000). The stable carbon isotope ratio ($\delta^{13}C$) compositions of the whole oils range from –28.5‰ to –24.3‰, with an average of –26.3‰ (Table 1). The $\delta^{13}C$ values of the saturates and aromatic hydrocarbons range from –29.3‰ to –25.1‰ and –28.0‰ to –23.4‰, with averages of –27.3‰ and –25.7‰, respectively. The oil samples in the study show relatively large variations in the $\delta^{13}C$, possibly because oils in the Zhanhua Depression were accumulated in different source rocks with complex palaeoenvironments and organic matter inputs.

4.2. GC fingerprints

Isoprenoids and *n*–alkanes are widely used in petroleum geochemistry (Peters et al., 2005), but they are significantly influenced by geochemical processes, especially biodegradation (Dong et al., 2015). Some oils in this study are influenced by biodegradation which caused lack of *n*–alkanes and unresolved complex mixture (UCM) (Fig. 2a). In contrast, other samples contain a full suite of apparently undegraded *n*–alkanes in the carbon number range of C_9 to C_{30+} (Fig. 2a). The carbon number distribution of *n*–alkanes are variable with maxima in the range of C_{17}–C_{23}. The ratios of $\sum n$–$C_{21-}/\sum n$–C_{22+} vary from 0.27 to 5.66, which was related to differences in depositional environment and maturity. The ratios of pristane to phytane (Pr/Ph) range from 0.28 to 1.92, the Pr/*n*–C_{17} and Ph/*n*–C_{18} ratios range in 0.26–3.67 and 0.20–2.63, respectively (Table 1). The relationships between Pr/*n*–C_{17} and Ph/*n*–C_{18} suggest significant differences in depositional environment and organic matter input of the source rocks for the crude oils. When we only take samples with complete *n*–alkanes and isoprenoids into consideration, the Pr/Ph ratios of the crude oils in Bonan–Gubei Sag are generally > 1(Table 1), consistent with source rocks deposited under oxic to suboxic conditions. In contrast, crude oils produced from the Luojia–Chenjiazhuang High display lower Pr/Ph ratios (around 0.5)

Table 2
Ratios of biomarkers discussed in this study.

Well	C_{19}/ C_{23}TT	C_{22}/ C_{21}TT	C_{24}/ C_{23}TT	C_{24}Te/ C_{26}TT	C_{26}/ C_{25}TT	ETR	C_{29}H/ C_{30}H	C_{35}H/ C_{34}H	C_{31}HR/ C_{30}H	Ga/ C_{30}H	TT/ H	S/H	C_{29}Ts/ C_{29}H	C_{30}M/ C_{30}H	ααα 20R C_{27} %	ααα 20R C_{28} %	ααα 20R C_{29} %	C_{29}ααα20S/ (S + R)	C_{29}ββ□ (αα + ββ)	Ts/ (Tm + Ts)	diaC$_{27}$/ regC$_{27}$
Y28	0.63	0.33	0.81	1.56	1.04	0.16	0.47	0.72	0.21	0.06	0.05	0.31	0.27	0.08	0.26	0.27	0.47	0.57	0.55	0.46	0.099
Y123	0.42	0.34	0.76	1.23	1.21	0.16	0.41	0.59	0.23	0.03	0.04	0.15	0.26	0.09	0.27	0.27	0.46	0.53	0.50	0.49	0.083
Y943	0.49	0.29	0.66	1.17	1.34	0.15	0.36	0.55	0.26	0.06	0.08	0.21	0.54	0.09	0.32	0.23	0.45	0.55	0.49	0.63	0.105
YD261	0.37	0.26	0.76	0.85	1.32	0.16	0.44	0.61	0.21	0.04	0.07	0.24	0.23	0.10	0.29	0.31	0.40	0.50	0.47	0.44	0.073
Y94	0.50	0.29	0.83	0.94	1.24	0.16	0.36	0.62	0.26	0.08	0.08	0.35	0.60	0.09	0.31	0.29	0.39	0.44	0.40	0.67	0.065
Y284	0.65	0.25	0.85	0.88	1.24	0.19	0.43	0.51	0.20	0.03	0.07	0.23	0.30	0.08	0.24	0.32	0.44	0.61	0.51	0.57	0.108
Y104	0.62	0.09	0.83	0.60	1.20	0.26	0.48	0.51	0.25	0.07	0.38	0.69	0.99	0.08	0.25	0.31	0.44	0.63	0.53	0.81	0.220
Y170	0.35	0.11	0.79	1.15	1.00	0.26	0.59	0.91	0.24	0.15	0.23	0.60	0.28	0.11	0.30	0.28	0.42	0.56	0.52	0.49	0.242
YG78	0.33	0.30	0.83	1.29	1.04	0.13	0.50	0.86	0.24	0.06	0.04	0.20	0.21	0.08	0.31	0.25	0.44	0.52	0.49	0.41	0.051
YG50	0.33	0.31	0.84	1.31	1.09	0.12	0.50	0.84	0.24	0.06	0.04	0.20	0.19	0.08	0.31	0.26	0.43	0.52	0.49	0.41	0.047
YG32	0.40	0.36	0.78	1.30	1.13	0.13	0.45	0.61	0.25	0.03	0.04	0.16	0.22	0.08	0.32	0.26	0.42	0.52	0.47	0.46	0.072
YG99	0.36	0.31	0.75	1.30	1.13	0.12	0.50	0.78	0.24	0.06	0.04	0.20	0.19	0.08	0.31	0.26	0.43	0.51	0.49	0.41	0.075
YD11	0.32	0.42	0.67	1.57	1.16	0.11	0.50	0.81	0.26	0.04	0.04	0.17	0.25	0.08	0.32	0.26	0.42	0.51	0.50	0.47	0.058
Y71	0.25	0.25	0.82	1.27	1.06	0.12	0.55	0.73	0.25	0.05	0.03	0.20	0.13	0.08	0.34	0.26	0.40	0.49	0.44	0.31	0.041
Y85	0.37	0.28	0.80	1.02	1.12	0.13	0.45	0.65	0.22	0.09	0.05	0.22	0.20	0.09	0.34	0.29	0.37	0.47	0.41	0.40	0.061
Y99	0.21	0.24	0.77	1.63	1.02	0.08	0.51	1.04	0.22	0.06	0.03	0.17	0.18	0.08	0.32	0.24	0.44	0.49	0.45	0.33	0.049
Y171	0.26	0.21	0.76	1.80	0.94	0.19	0.78	1.01	0.25	0.09	0.13	0.49	0.17	0.07	0.29	0.29	0.41	0.58	0.53	0.34	0.125
YD341	0.32	0.30	0.78	1.85	1.05	0.17	0.56	0.74	0.27	0.06	0.10	0.27	0.26	0.07	0.26	0.32	0.43	0.54	0.51	0.53	0.063
YG79	0.26	0.30	0.80	1.95	0.84	0.09	0.55	1.11	0.23	0.11	0.04	0.25	0.15	0.07	0.37	0.25	0.38	0.40	0.38	0.30	0.050
Y88	0.27	0.21	0.67	0.84	1.20	0.14	0.44	0.62	0.21	0.25	0.04	0.29	0.18	0.09	0.37	0.32	0.31	0.34	0.31	0.37	0.072
Y50	0.19	0.12	0.63	0.51	1.15	0.25	0.33	0.65	0.20	0.42	0.12	0.53	0.28	0.09	0.31	0.32	0.38	0.44	0.39	0.47	0.044
B71	0.33	0.23	0.69	0.90	1.19	0.21	0.39	0.58	0.24	0.12	0.08	0.26	0.47	0.10	0.31	0.30	0.40	0.51	0.42	0.59	0.090
BY1	0.26	0.21	0.68	1.04	1.14	0.16	0.49	0.93	0.25	0.17	0.06	0.27	0.21	0.10	0.36	0.30	0.34	0.39	0.37	0.36	0.056
B55	0.27	0.23	0.68	1.08	1.08	0.13	0.53	1.13	0.25	0.16	0.06	0.20	0.21	0.11	0.30	0.27	0.42	0.42	0.42	0.34	0.129
BG602	0.21	0.13	0.73	1.28	1.23	0.11	0.59	0.67	0.25	0.08	0.02	0.54	0.20	0.16	0.31	0.31	0.38	0.17	0.15	0.28	0.067
GBG2	0.66	0.18	0.88	0.69	1.12	0.17	0.41	0.73	0.26	0.07	0.20	0.40	1.08	0.11	0.31	0.31	0.39	0.64	0.51	0.78	0.189
GB210	0.37	0.24	0.74	1.18	1.27	0.11	0.53	0.69	0.24	0.07	0.06	0.22	0.25	0.12	0.38	0.23	0.40	0.40	0.37	0.39	0.069
GB351	0.43	0.25	0.69	0.98	1.22	0.16	0.40	0.66	0.26	0.05	0.07	0.22	0.45	0.10	0.32	0.27	0.41	0.55	0.46	0.58	0.097
GB391	0.43	0.29	0.72	1.07	1.02	0.14	0.40	0.59	0.25	0.04	0.06	0.21	0.45	0.10	0.33	0.26	0.41	0.55	0.46	0.57	0.094
Z130	0.32	0.28	0.71	1.31	1.14	0.17	0.50	0.93	0.26	0.11	0.05	0.22	0.20	0.08	0.36	0.26	0.38	0.30	0.42	0.38	0.124
Z183	0.32	0.26	0.70	1.19	1.13	0.18	0.48	0.84	0.24	0.19	0.05	0.31	0.20	0.10	0.38	0.28	0.34	0.22	0.34	0.35	0.122
Z194	0.32	0.26	0.66	1.26	1.06	0.17	0.51	0.94	0.25	0.19	0.05	0.28	0.17	0.10	0.37	0.28	0.35	0.23	0.39	0.31	0.123
Z164	0.37	0.25	0.70	1.18	1.13	0.16	0.47	0.79	0.24	0.19	0.05	0.28	0.19	0.11	0.37	0.28	0.35	0.25	0.34	0.35	0.116
Z190	0.31	0.25	0.67	1.23	1.15	0.17	0.48	0.86	0.25	0.17	0.05	0.28	0.20	0.10	0.36	0.29	0.35	0.26	0.36	0.36	0.129
Z501	0.33	0.24	0.69	1.20	1.18	0.17	0.49	0.86	0.25	0.20	0.04	0.29	0.19	0.11	0.37	0.28	0.35	0.26	0.35	0.35	0.120
Z187	0.35	0.24	0.67	1.19	1.13	0.17	0.47	0.88	0.24	0.18	0.05	0.29	0.19	0.10	0.37	0.28	0.35	0.27	0.34	0.36	0.123
Z48	0.35	0.26	0.69	1.21	1.13	0.17	0.50	0.76	0.25	0.20	0.05	0.27	0.17	0.10	0.37	0.28	0.35	0.26	0.35	0.33	0.108
Z452	0.31	0.24	0.66	1.19	1.14	0.17	0.50	0.94	0.24	0.21	0.05	0.32	0.17	0.09	0.37	0.27	0.36	0.25	0.30	0.35	0.109
Z198	0.30	0.26	0.67	1.20	1.12	0.17	0.51	1.00	0.26	0.22	0.05	0.31	0.18	0.10	0.36	0.29	0.35	0.27	0.34	0.32	0.113
Z45	0.30	0.25	0.67	1.17	1.17	0.16	0.50	0.88	0.25	0.23	0.04	0.31	0.18	0.11	0.36	0.29	0.35	0.26	0.33	0.34	0.118
Z29	0.31	0.26	0.66	1.21	1.14	0.17	0.49	0.86	0.25	0.20	0.05	0.28	0.18	0.10	0.37	0.29	0.35	0.28	0.35	0.35	0.134
Z195	0.27	0.28	0.65	1.16	1.22	0.15	0.50	0.99	0.26	0.22	0.04	0.30	0.17	0.10	0.37	0.28	0.35	0.26	0.39	0.29	0.106
Z9	0.19	0.24	0.62	1.43	1.13	0.11	0.52	1.07	0.26	0.20	0.04	0.33	0.03	0.01	0.38	0.29	0.33	0.34	0.35	0.32	0.031
Z11	0.18	0.24	0.61	1.47	1.03	0.11	0.52	1.13	0.27	0.21	0.04	0.30	0.16	0.09	0.39	0.28	0.32	0.48	0.40	0.33	0.031
Z200	0.18	0.33	0.53	1.41	1.00	0.14	0.52	1.40	0.27	0.24	0.05	0.33	0.13	0.08	0.35	0.29	0.37	0.20	0.31	0.24	0.081
D40	0.41	0.25	0.82	1.59	1.20	0.13	0.52	1.28	0.19	0.21	0.05	0.65	0.20	0.08	0.34	0.23	0.43	0.53	0.52	0.34	0.063
D677	0.14	0.15	0.62	1.34	1.09	0.09	0.53	1.01	0.21	0.06	0.03	0.24	0.15	0.12	0.39	0.24	0.37	0.39	0.27	0.23	0.057
KG2	0.30	0.19	0.73	1.15	1.07	0.19	0.53	0.59	0.22	0.03	0.05	0.19	0.23	0.12	0.33	0.25	0.42	0.38	0.37	0.39	0.177
K37	0.41	0.28	0.73	1.22	1.20	0.15	0.44	0.64	0.22	0.03	0.06	0.23	0.32	0.11	0.36	0.26	0.38	0.43	0.39	0.49	0.054
KG65	0.29	0.29	0.69	1.18	1.15	0.17	0.50	0.81	0.27	0.09	0.05	0.20	0.21	0.10	0.35	0.28	0.37	0.34	0.43	0.39	0.125
K26	0.16	0.23	0.64	1.90	1.02	0.09	0.62	1.21	0.36	0.05	0.03	0.17	0.12	0.07	0.36	0.25	0.39	0.47	0.46	0.26	0.046
GN210	0.24	0.24	0.70	1.15	1.16	0.12	0.52	0.97	0.28	0.09	0.04	0.21	0.16	0.09	0.34	0.27	0.39	0.44	0.42	0.37	0.052

(*continued on next page*)

Table 2 (*continued*)

Well	$C_{19}/C_{23}TT$	$C_{22}/C_{21}TT$	$C_{24}/C_{23}TT$	$C_{24}Te/C_{26}TT$	$C_{26}/C_{25}TT$	ETR	$C_{29}H/C_{30}H$	$C_{35}H/C_{34}H$	$C_{31}HR/C_{30}H$	Ga/$C_{30}H$	TT/H	S/H	$C_{29}Ts/C_{29}H$	$C_{30}M/C_{30}H$	ααα 20R C_{27} %	ααα 20R C_{28} %	ααα 20R C_{29} %	$C_{29}ααα20S/(S+R)$	$C_{29}ββ□(αα+ββ)$	Ts/(Tm + Ts)	$diaC_{27}/regC_{27}$
GN211	0.27	0.23	0.72	1.16	1.12	0.13	0.51	0.83	0.25	0.09	0.04	0.23	0.18	0.09	0.36	0.28	0.36	0.43	0.42	0.39	0.066
GN363	0.19	0.12	0.54	0.73	1.32	0.19	0.38	0.62	0.23	0.36	0.08	0.52	0.34	0.11	0.37	0.31	0.32	0.36	0.27	0.44	0.082
KX626	0.12	0.36	0.52	1.80	1.20	0.02	0.63	2.34	0.30	0.20	0.03	0.33	0.11	0.07	0.36	0.24	0.39	0.37	0.54	0.80	0.018
YG4	0.12	0.12	0.69	1.12	1.04	0.14	0.45	0.98	0.28	0.41	0.05	0.53	0.15	0.08	0.39	0.34	0.27	0.27	0.25	0.27	0.013
L354	0.16	0.38	0.58	1.88	1.03	0.09	0.54	1.34	0.41	0.08	0.02	0.17	0.09	0.07	0.37	0.23	0.40	0.29	0.45	0.20	0.052
L358	0.19	0.32	0.63	2.23	1.15	0.11	0.53	2.16	0.22	0.45	0.05	0.74	0.14	0.08	0.38	0.22	0.40	0.42	0.53	0.09	0.027
L321	0.11	0.39	0.51	2.21	1.24	0.08	0.59	2.09	0.28	0.41	0.04	0.48	0.11	0.06	0.36	0.22	0.43	0.39	0.51	0.08	0.023
C312	0.18	0.20	0.59	1.57	1.09	0.10	0.57	1.40	0.29	0.16	0.04	0.27	0.14	0.08	0.36	0.26	0.38	0.44	0.43	0.28	0.062
C48	0.16	0.20	0.57	1.77	0.92	0.09	0.60	1.56	0.30	0.20	0.04	0.26	0.12	0.08	0.37	0.28	0.36	0.33	0.49	0.24	0.069
C375	0.15	0.21	0.58	1.86	1.01	0.10	0.64	1.64	0.30	0.18	0.04	0.27	0.11	0.07	0.37	0.27	0.37	0.32	0.50	0.24	0.070
C163	0.12	0.13	0.59	1.47	1.08	0.08	0.54	1.39	0.32	0.24	0.03	0.34	0.12	0.08	0.37	0.30	0.33	0.27	0.32	0.21	0.066
C16	0.09	0.15	0.59	2.86	1.29	0.07	0.55	1.53	0.32	0.25	0.03	0.35	0.10	0.07	0.38	0.30	0.31	0.31	0.35	0.19	0.063
C162	0.06	0.11	0.51	1.76	1.09	0.06	0.50	2.06	0.33	0.31	0.03	0.37	0.09	0.07	0.37	0.27	0.36	0.49	0.45	0.10	0.054

Note: $C_{24}Te/C_{26}TT$=C_{24} tetracyclic terpane/C_{26} 22(S + R) tracyclic terpane, ETR=($C_{28}TT + C_{29}TT$)/($C_{28}TT + C_{29}TT + Ts$), $C_{29}H/C_{30}H$=C_{29} hopane/C_{30} hopane, $C_{35}H/C_{34}H$=C_{35} pentakishomohopane 22(S + R)/C_{34} tetrakishomohopane, $C_{31}HR/C_{30}H$=C_{31} homohopane 22R/C_{30} hopane, Ga/$C_{30}H$ = gammacerane/C_{30} hopane, TT/H=$\sum C_{19\text{-}30}TT/\sum C_{29\text{-}35}$ hopane, S/H = sterane/hopane=$\sum C_{27\text{-}29}$ steranes/$\sum C_{29\text{-}35}$ hopane, ααα 20R = 5α,14α,17α(H)-cholestane 20R, $C_{29}Ts$ = 18α(H)-30-norneohopane, $C_{30}M/C_{30}H$ = 17β(H),21α(H)-moretane/17α(H),21β(H)-hopane, $C_{29}ααα20S$ = C_{29}5α,14α,17α(H) –stigmastane 20S, $C_{29}ααα20R$ = C_{29}5α,14α,17α(H) –stigmastane 20R, $C_{29}ββ$ = [C_{29}5α,14β,17β(H)-stigmastane 20S] + [C_{29}5α,14β,17β(H)-stigmastane 20R], $diaC_{27}$ = C_{27}13β,17α(H) –diacholestane.

consistent with source rocks deposited in a highly saline and reducing depositional environment (Hunt, 1996; Harris et al., 2004).

4.3. Biodegradation

Several samples in this study have undergone biodegradation, thus, the effect of biodegradation should be addressed first. Generally, 25–norhopane identified by m/z = 177 mass chromatograms is an indicator of severe biodegradation (Blance and Connan, 1992; Peters et al., 1997). In most investigated oils from the Zhanhua Depression, the entire series of 25–norhopane (25 N–Hs), including C_{29}–and C_{28}–norhopanes, C_{30-34}–norhomohopanes, C_{27}–nortrinorhopanes, and 17–nortricyclic terpanes, is identified with different abundances (Fig. 2b). The 25 N–$C_{29}H/C_{30}H$ ratios range from 0.02 to 0.14 (Table 1), suggesting severe biodegradation has occurred (Peters and Moldowan, 1993). Many oil samples in this study lack in *n*–alkanes, however, many crudes with elevated 25 N–$C_{29}H/C_{30}H$ ratios also appear to contain the complete set of undegraded steranes and pentacyclic triterpanes (hopanes), obviously that is not in keeping with the proposed quasi–-stepwise removal of compound classes that accompanies biodegradation (Peters and Moldowan, 1993). We suggest that the most likely explanation for this apparent discrepancy is that the crudes in the Zhanhua Depression are the result of multi–period charge. The early expelled crudes accumulated in Ed formation were subsequently biodegraded in the reservoirs (Zhang et al., 2007), leaving only the 25–norhopanes and asphaltic components from that original oil phase. These severely degraded crudes were subsequently mixed with oils from Ng and Mz formations that remained undegraded or experienced only mild microbial alteration (Zhao et al., 2000; Guo et al., 2001). Oils accumulated in later stage have undergone slight biodegradation, the biodegradation of the samples is below level 4, whereby the *n*–alkanes and isoprenoids were altered or completely removed, but the hopanes and steranes remain largely unaffected.

4.4. Biomarker composition and distribution

4.4.1. Terpenoids

Terpenoid hydrocarbons were measured using m/z 191 mass chromatograms, and the parameters are shown in Table 2 and Fig. 3a. The terpane traces of the crude oils from the Zhanhua Depression are similar, with a predominance of pentacyclic triterpanes and low abundances of the tricyclic terpanes (TT). The main tricyclic terpanes peak is $C_{23}TT$. The ratios of $C_{19}TT/C_{23}TT$ (0.19–0.66, with an average of 0.37) in crude oils produced in the Bonan–Gubei Sag are relatively high compared to the Luojia–Chenjiazhuang High (average at 0.13, Fig. 4a). Pentacyclic terpanes are dominated by $C_{30}H$ in all samples. The ratios of $C_{29}H/C_{30}H$ range from 0.33 to 0.78 (Table 2). $C_{29}Ts/C_{29}H$ ratios range from 0.03 to 1.08, average at 0.32 and 0.11 in oils from the Bonan–Gubei Sag and Luojia–Chenjiazuang High, respectively (Fig. 5b). The relatively high $C_{26}/C_{25}TT$ (0.84–1.34) and low $C_{31}R/C_{30}H$ (0.20–0.27) ratios suggest that the oils were derived from lacustrine source rocks (Aquino Neto et al., 1983). The relative intensities of C_{31}–C_{35} homohopanes decrease with increasing carbon number in most samples from the Bonan–Gubei Sag. The $C_{35}H/C_{34}H$ ratios range from 0.51 to 1.13, with an average of 0.74 (Fig. 5a). The C_{35} homohopanes are present in higher abundance than the C_{34} homohopanes ($C_{35}H/C_{34}H$ ratios range from 0.98 to 2.34, with an average of 1.68) in most samples from the Luojia–Chenjiazuang High. The gammacerane concentrations are low in the Bonan–Gubei Sag (the $Ga/C_{30}H$ ratios vary from 0.03 to 0.42, with an average of 0.09.), while they are relatively high in the Luojia–Chenjiazuang High (the $Ga/C_{30}H$ ratios average at 0.26). The $C_{35}H/C_{34}H$ and $Ga/C_{30}H$ ratios indicating the source rocks were deposited in different redox, salinity and water–column stratification (Peters et al., 2005). The abundances of 17α(H)–trisnorneohopane (Tm) and 18α(H) trisnorneohopane (Ts) are relatively low, the Ts/(Ts + Tm) ratios range from 0.08 to 0.81 (Fig. 6b), suggesting the oils were generated in the early to peak oil window

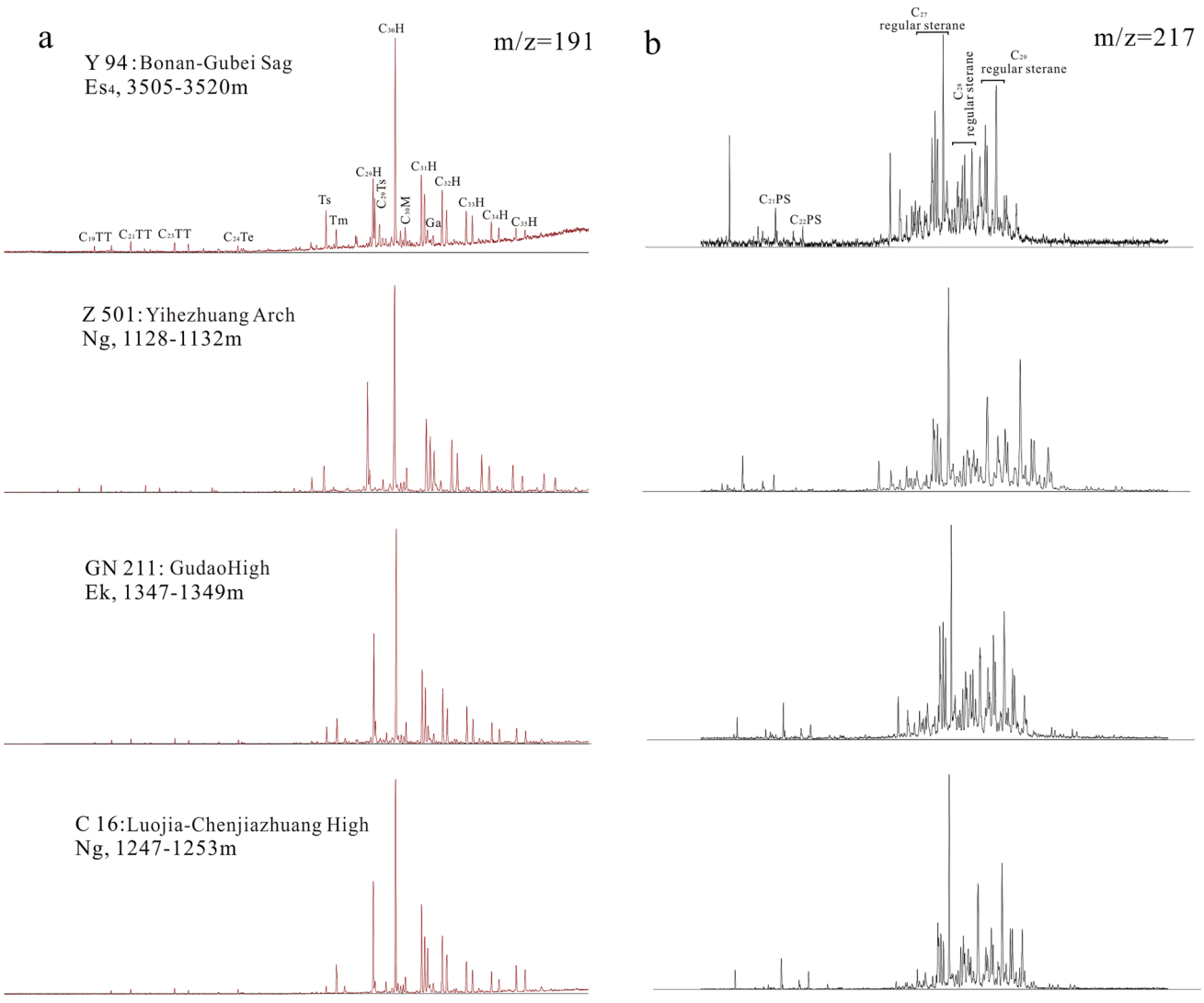

Fig. 3. Representative *m/z* 191 (a) and *m/z* 217 (b) mass chromatograms showing the terpane and sterane distributions, respectively. Y94, Z501, GN211 and C16 was collected from Bonan–Gubei Sag, Yihezhuang Arch, Gudao High and Luojia–Chenjiazhuang High, respectively. Note: TT = tricyclic terpane, C_{24}Te = C_{24} tetracyclic terpane, H = hopane or homohopane, Ts = C_{27}18α(H) 22,29,30–trisnorhopane, Tm = C_{27}17α(H) 22,29,30–trisnorhopane, C_{29}Ts = 18α(H)–30–norneohopane, C_{29}H = C_{29}17α(H),21β(H)–30–norhopane, C_{30}M = 17β(H),21α(H)–moretane, C_{30}H = 17α (H),21β (H)–hopane.

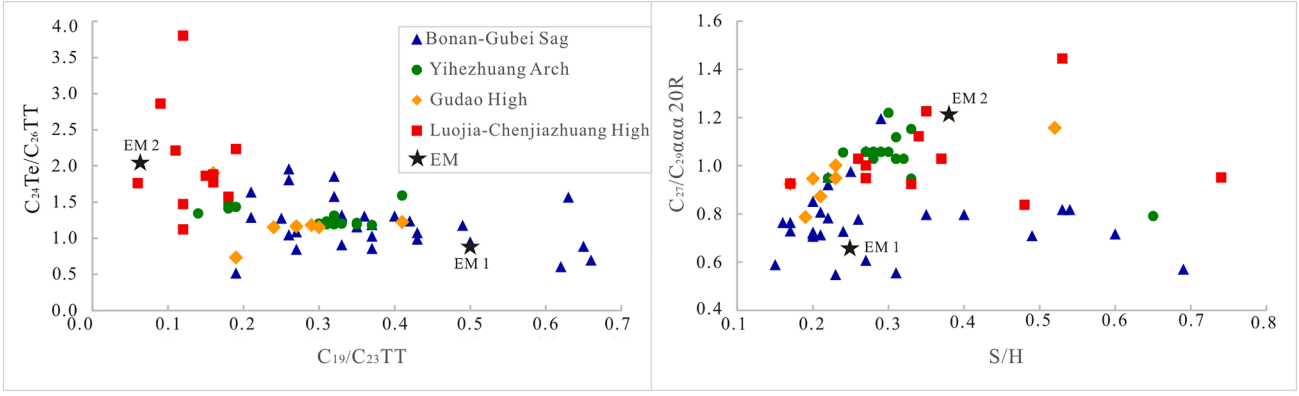

Fig. 4. Correlations of the source–related ratios of (a) C_{19}/C_{23}TT vs. C_{24}Te/C_{26}TT and (b) S/H vs. C_{27}/C_{29} ααα20R, showing the interpreted differences in organic matter input of the source rocks for the crude oils in different geographic area. Compound symbols are described in the footnotes of the Table 2 and Fig. 3.

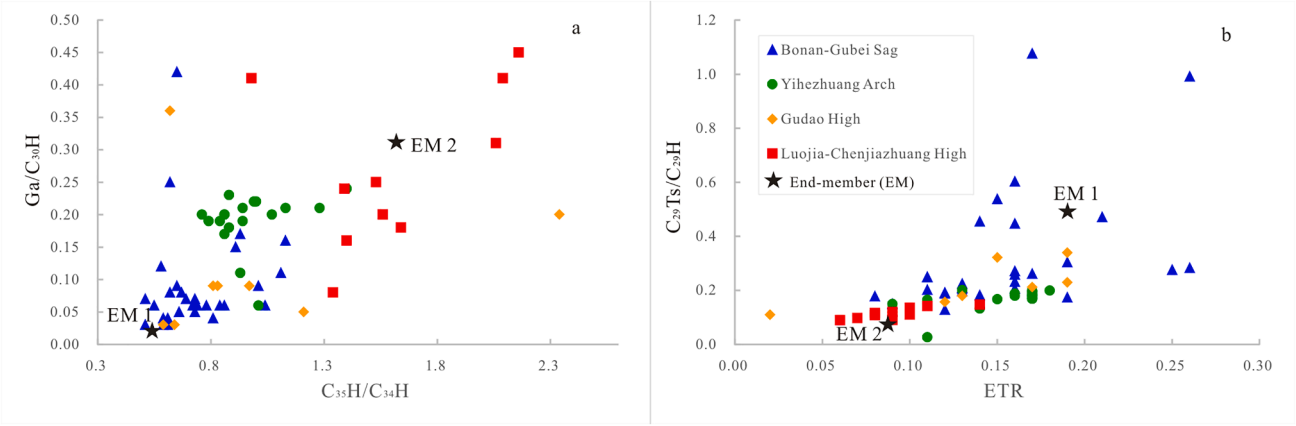

Fig. 5. Correlations of the depositional environment–related ratios of (a) C_{35}/C_{34} vs. $Ga/C_{30}H$ and (b) ETR vs. $C_{29}Ts/C_{29}H$, showing the interpreted differences in depositional redox conditions of the source rocks for the crude oils in different geographic area. Compound symbols are described in the footnotes of the Table 2 and Fig. 3.

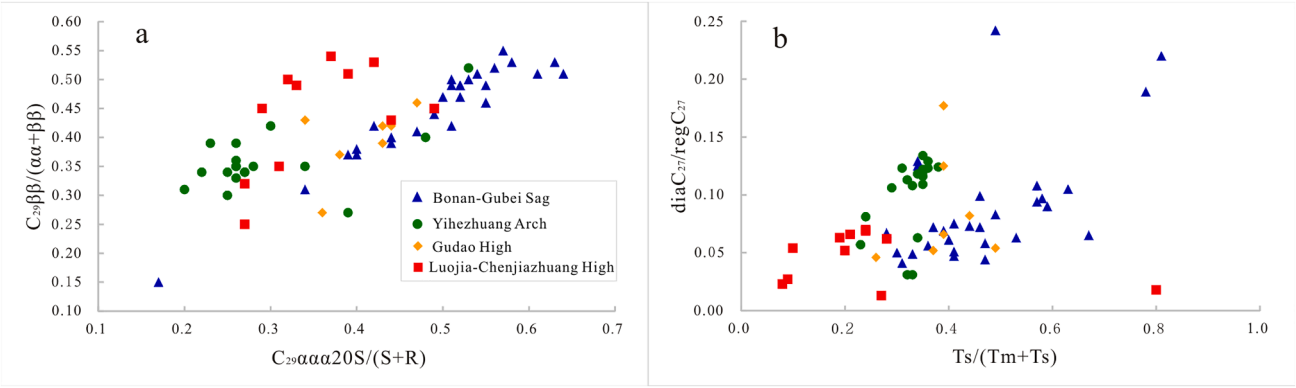

Fig. 6. Correlations of the maturation–related ratios of (a) $C_{29}ααα20S/(20S + 20R)$ vs. $C_{29}ββ/(αα + ββ)$ and (b) $Ts/(Ts + Tm)$ vs. $diaC_{27}/regC_{27}$, showing the variations in maturity of the crude oils in different geographic area. Compound symbols are described in the footnotes of the Table 2 and Fig. 3.

(Farrimond et al., 1996).

4.4.2. Steroids

The *m/z* 217 mass chromatograms reveal the sterane distributions of the samples. The pregnanes and diasteranes are present in all samples at low abundances compared to regular steranes (Fig. 3b). The distributions of the regular steranes $C_{27}ααα(20R)$, $C_{28}ααα(20R)$, and $C_{29}ααα(20R)$ indicate asymmetric "V–type" distributions. The relative abundances of C_{27}, C_{28}, and C_{29} steranes range from 24% to 39%, 22%–34%, and 27%–47%, respectively. In most samples from the Bonan–Gubei Sag, the C_{27}/C_{29} ααα 20R sterane ratios are below 1.00 (Fig. 4b), and S/H ratios are generally low (average at 0.29), indicating terrestrial organic matter input for the source rock (Peters et al., 2005). For samples in the Luojia–Chenjiazhuang High, the C_{27}/C_{29} ααα 20R sterane ratios range from 0.83 to 1.44 (Fig. 4b, Table 2) and average at 1.05, the S/H ratios are average at 0.37, suggesting the contribution of microalga to the source rock (Peters et al., 2005). The C_{27} diasteranes are present in low abundance relative to the regular steranes with $diaC_{27}/regC_{27}$ ratios between 0.01 and 0.24 (Fig. 6b). The $C_{29}20S/(20S + 20R)$ and $C_{29}ββ/(αα + ββ)$ ratios range from 0.17 to 0.64 and 0.15–0.55 (Fig. 6a), respectively, suggesting that the investigated oils were generated in the early to peak oil window stages (Hanson, 2000; Peters and Moldowan, 1993) which is corresponds to $Ts/(Ts + Tm)$.

Table 3
Parameters of the end–members calculated by ALS.

Parameter	EM1	EM2
$\delta^{13}C_{Oil.}$ /‰	−26.0	−26.5
$\delta^{13}C_{Sat.}$ /‰	−25.6	−28.4
$\delta^{13}C_{Aro.}$ /‰	−24.8	−26.1
$C_{19}/C_{23}TT$	0.50	0.06
$C_{22}/C_{21}TT$	0.27	0.22
$C_{24}/C_{23}TT$	0.83	0.53
$C_{24}Te/C_{26}TT$	0.84	1.99
ETR	0.19	0.09
$C_{29}H/C_{30}H$	0.44	0.57
$C_{35}/C_{34}H$	0.51	1.69
$C_{31}HR/C_{30}H$	0.23	0.30
$Ga/C_{30}H$	0.03	0.31
TT/H	0.10	0.02
S/H	0.25	0.38
$C_{29}Ts/C_{29}H$	0.49	0.09
$C_{30}M/C_{30}H$	0.11	0.07
ααα 20R C_{27} %	29%	40%
ααα 20R C_{28} %	28%	27%
ααα 20R C_{29} %	43%	33%
Sedimentary environment	Freshwater–brackish, non–stratified water column, weakly reducing conditions	Hypersaline, stratified water column with strongly reducing bottom water
Organic matter input	Combined microalgal material and terrestrial organic matter	Microalgal/bacterial
Inferred setting	Es_3^L shale	Es_4^U shale

Table 4
Results of the multivariate statistical analysis.

Well	ALS result		MDS result	
	EM1	EM2	MDS1	MDS2
Y28	90%	10%	−0.18	0.17
Y123	92%	8%	−0.21	0.16
Y943	80%	20%	−0.15	0.2
YD261	82%	18%	−0.17	0.01
Y94	92%	8%	−0.21	0.02
Y284	100%	0%	−0.31	0.05
Y104	100%	0%	−0.31	−0.12
Y170	74%	26%	−0.15	−0.1
YG78	83%	17%	−0.1	0.18
YG50	81%	19%	−0.1	0.16
YG32	82%	18%	−0.14	0.16
YG99	78%	22%	−0.1	0.14
YD11	72%	28%	−0.07	0.22
Y71	66%	34%	−0.03	0.15
Y85	74%	26%	−0.11	0.06
Y99	58%	42%	0.02	0.22
Y171	62%	38%	−0.11	−0.08
YD341	91%	9%	−0.24	0.11
YG79	58%	42%	0.04	0.3
Y88	49%	51%	−0.01	−0.1
Y50	57%	43%	−0.09	−0.22
B71	70%	30%	−0.11	−0.01
BY1	54%	46%	−0.04	−0.02
B55	56%	44%	0.01	0.11
BG602	51%	49%	−0.02	−0.18
GBG2	93%	7%	−0.22	−0.06
GB210	64%	36%	−0.04	0.17
GB351	85%	15%	−0.17	0.08
GB391	82%	18%	−0.16	0.12
Z130	57%	43%	−0.03	0.1
Z183	50%	50%	0	−0.03
Z194	48%	52%	0.01	0.04
Z164	53%	47%	−0.03	0.01
Z190	51%	49%	−0.01	0
Z501	50%	50%	0.01	0.02
Z187	50%	50%	0	0.01
Z48	52%	48%	−0.01	0.03
Z452	45%	55%	0.03	0.03
Z198	46%	54%	0.03	0.01
Z45	47%	53%	0.02	0
Z29	48%	52%	0.01	0.01
Z195	40%	60%	0.05	0.01
Z9	34%	66%	0.08	−0.01
Z11	29%	71%	0.1	0
Z200	30%	70%	0.12	0.03
D40	55%	45%	0.06	0.22
D677	33%	67%	0.15	0.15
KG2	84%	16%	−0.14	0.25
K37	83%	17%	−0.19	0.12
KG65	57%	43%	−0.03	0.06
K26	40%	60%	0.11	0.21
GN210	52%	48%	0.02	0.1
GN211	55%	45%	−0.01	0.07
GN363	36%	64%	0.04	−0.2
KX626	5%	95%	0.27	0.19
YG4	25%	75%	0.11	−0.15
L354	37%	63%	0.14	0.26
L358	11%	89%	0.26	0.1
L321	7%	93%	0.3	0.15
C312	29%	71%	0.12	0.08
C48	18%	82%	0.17	0.03
C375	21%	79%	0.16	0.06
C163	19%	81%	0.17	−0.05
C16	0%	100%	0.25	−0.08
C162	0%	100%	0.29	−0.02

4.5. Oil–oil correlation based on chemometrics

4.5.1. ALS deconvolution

The biomarker characteristics of oils collected in different tectonic units vary considerably (Fig. 4, Fig. 5). Even in the same area, the biomarker parameters associated with the palaeoenvironment, paleosalinity, and maturity show significantly variation, due to the varying contributions of different source rocks to the oils. In this study, in order to evaluate quantitatively the relative contribution from each source rock to the mixed oils in the Zhanhua Depression, we calculated the number of the EM for the mixture oils and the biomarker ratios of the EMs using ALS. The number of EM (maximum sources) of the mixed oil samples from the Zhanhua Depression was identified as two based on ALS and geological considerations. The cumulative variance is 93.0% by two EMs in ALS, following the requirements of multivariate statistical analysis (generally > 90%). The biomarker ratios of the two EMs calculated by ALS are listed in Table 3 and the relative contributions of the two EMs to Zhanhua Depression oils are listed in Table 4.

The EM1 is characterized by relatively low abundance of gammacerane ($Ga/C_{30}H$ = 0.03), a relatively high abundance of the $C_{29}Ts$ relative to $C_{29}H$ ($C_{29}Ts/C_{29}H$ = 0.49), the relative intensities of C_{31}–C_{35} homohopanes decrease with increasing carbon number ($C_{35}/C_{34}H$ = 0.51), relatively low abundances of steranes (S/H = 0.25), distribution of ααα steranes dominated by the C_{29} sterane with lesser but near equal abundances of the C_{27} and C_{28} sterane, and its $C_{19}/C_{23}TT$ ratio being 0.50 (Table 3; Fig. 4,5). A high C_{35} homohopane concentration is interpreted as general indicator of highly reducing conditions during deposition (Peters and Moldowan, 1991; Peters et al., 2005). The presence of high gammacerane is an indicator of water column stratification that often is the result of highly saline environments (Sinninghe Damste et al. 1995; Summons et al., 2008; Albaghdady, 2013). The formation of $C_{29}Ts$ is inhibited in reducing environment (Moldowan et al., 1991). The C_{27} steranes are believed to originate from phytoplankton, metazoans and other species of algae, while C_{29} steranes are often associated with terrestrial higher plants (Volkman, 1986; Hunt, 1996; Peters et al., 2005). Elevated $C_{19}TT$ indicate important contribution of terrestrial organic matter (Volkman, 1986; Holba et al., 2003; Cheng et al., 2018). The S/H ratio indicate input of eukaryotic vs prokaryotic organisms (microalgae and higher plants vs bacteria) to source rocks (Holba et al., 2003; Peters et al., 2005; Zhan et al., 2019). Collectively these parameters of EM1 suggest the deposition of microalgal material combined with terrigenous organic matter in a suboxic environment. In contrast, the EM2 is characterized by higher abundance of gammacerane, relatively low values of $C_{19}/C_{23}TT$ (0.06) and $C_{29}Ts/C_{30}H$ (0.09), a partial reversal of the distributions of $C_{31}H$ to $C_{35}H$ ($C_{35}/C_{34}H$ = 1.69), ααα sterane distributions are dominated by the C_{27} sterane and elevated S/H ratio (0.38) compared to EM1. The molecular parameters of EM2 are consistent with deposition of microalgae organic matter in anoxic environment.

As shown by Shi et al. (2005), Zhang et al. (2015), and Zhang et al. (2009) the extracts of the Es_4^U source rocks in the Zhanhua Depression are characterised by low Pr/Ph ratios (less than0.75) and relative high $Ga/C_{30}H$ (0.2–0.8), $C_{35}H/C_{34}H$ (>1.0), C_{27}/C_{29} ααα 20R sterane (>1.0) ratios. The Es_3^L shale has variable Pr/Ph ratios (0.7–1.7), a low $Ga/C_{30}H$ ratio (less than0.2), and almost equal abundances of C_{27}, C_{28}, and C_{29} steranes. Based on these data and other research (Cai et al., 2005; Hao et al., 2009; Jiu et al., 2013; Lu et al., 2012; Zhang et al., 2007; Zhan et al., 2019), the Es_4^U shale was mainly deposited in a saline semi–deep lacustrine environment with microalgal organic matter, and the Es_3^L shale was mainly deposited in freshwater–brackish lacustrine environments with a combination of microalgae material and terrigenous organic input. The Es_4^U shale has a higher salinity and more reducing deposit condition than the Es_3^L shale. Therefore, we speculate that EM1 represents the Es_3^L shale, while EM2 represents the Es_4^U shale.

The results obtained from ALS deconvolution demonstrate that EM1 is the dominate contributor for crude oils from the Bonan–Gubei Sag, accounting for 49%–100%, with an average of 75% (Table 4). The contribution of EM2 ranges from 0% to 51%. For oils in the Yihezhuang Arch, the contribution of EM1 ranges from 29% to 57%, while the contribution of EM2 varies from 42% to 70%. With respect to samples from the Gudao High, the contribution of EM1 ranges from 36% to 84% and the contribution of EM2 ranges from 15% to 63%. The EM2 is the

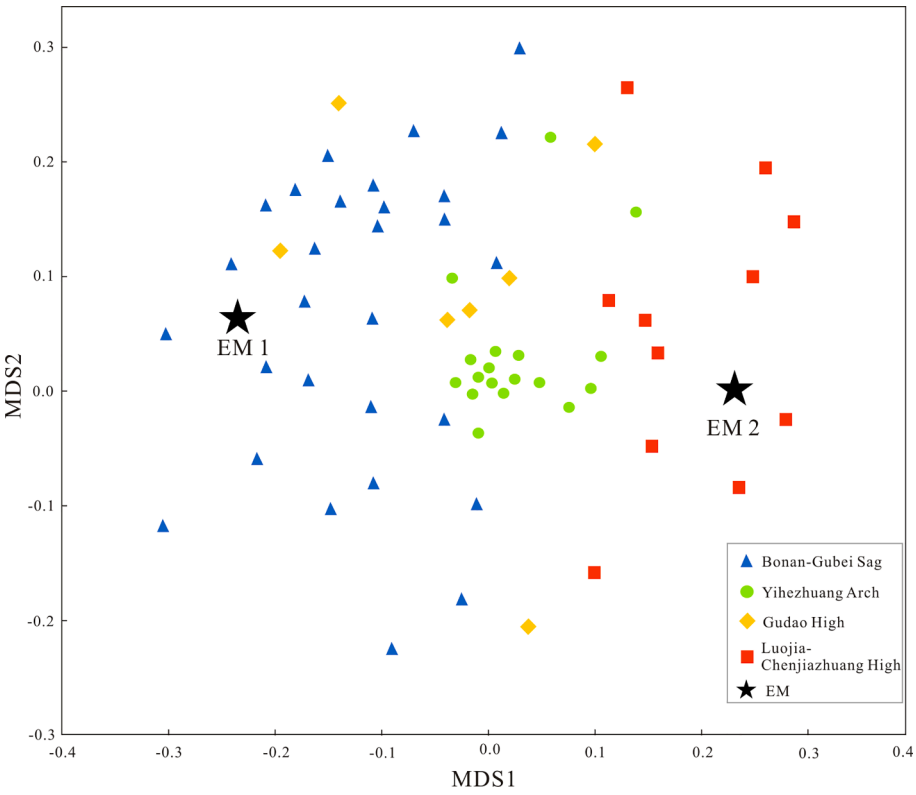

Fig. 7. MDS plot for oils and EMs calculated using ALS, the plane distance between the samples represents the similarity and divergence of the crude oils.

major contributor for oils from the Luojia–Chenjiazhuang High, with proportions in the range of 63%–100%.

Based on the description of Zhang et al. (2015), oils from the Bonan Sag and Gubei Sag mainly come from Es_3^L shale, oils from the Luojia Nose and Chenjiazhuang High mainly come from Es_4^U shale, oils from the Gudao High were the mixture of Es_3^L shale and Es_4^U shale, oils in the east of the Yihezhuang Arch were from Es_1 shale. Our calculation result of ALS was basically consistent with previous research, but we found that oils in the east of Yihezhuang Arch were the mixture of Es_3^L shale and Es_4^U shale. It is known that most Es_1 shale has poor capacity of hydrocarbon generation with less thickness, low maturity and limited distribution (Zhan et al., 2019). This study gives a more accurate estimation of the contribution of Es_3^L shale and Es_4^U shale for the mixed oils in the Zhanhua Depression

4.5.2. Mds

MDS is an effective multivariate oil–oil and oil–source correlation tool, in which the Bray–Curtis distance is generally used to distinguish datasets based on the biomarker ratios of oils (Wang et al., 2018). The Standardized Residual Sum of Squares (SRESS) is a measure of the degree of the deviation of the best–fitting configuration from the original dataset. The original variance equation, $(1.0 - \text{STRESS}) \times 100\%$, can be used to measure the fitness degree of the best–fitting configuration representing the original dataset (Wang et al., 2018).

We applied three carbon isotope ratios and 16 biomarker ratios of the EMs and crude oil samples to compute the Bray–Curtis distance among samples and draw a two–dimensional (2D) MDS diagram using in–house software. In this study, the STRESS value of the MDS was 3.75% after 1000 iterations, the original variance is 96.25%, which results in the fitness degree ranging from good to excellent. The genetic relationships between the crude oil samples and EMs calculated by ALS can be easily distinguished in the 2D plot (Fig. 7). The EM1 has a close relationship with oils collected from the Bonan–Gubei Sag, and the EM2 has a close relationship with oils collected from the Luojia–Chenjiazhuang High. The distance between the samples reflects the affinity of the oil. Oils from the Yihezhuang Arch are closely clustered. Other oils from different tectonic units are closely clustered in terms of horizontal axis but dispersed in terms of vertical axis. Overall, the MDS results are consistent with the ALS results

4.5.3. Circos

Circos can automatically produce accurate linear representations of circular sequences (Martin et al., 2015). Circos is licensed by GPL, we chose an interactive online version, which is available at http://mkweb.bcgsc.ca/circos/tableviewer, to visualise the tabular data. In this study, we imported the ALS results into circos to visualise the relative contributions of EM1 and EM2 to oils. In addition, the total contribution of a given EM for a geographic area was estimated by circos. This method clarifies the relation between the source rocks and oils and calculates the volumetric charge of a given source rock to each geographic area.

As shown in Fig. 8, the length of arc AB and CD is proportional to the total contribution of EM2 and EM1 to oils in a tectonic unit, respectively. The relative contribution of the two EMs can be inferred from the arc length. Each segment on arc EF corresponds to the relative contribution of the two EMs in each oil sample. The colourful ribbons in the circle connect the EMs with oils. In Fig. 8a, the ratio of the length of arc CD to that of arc AB is 1.38, which means that the contribution of EM1 (Es_3^L) is slightly higher than that of EM2 (Es_4^U) in the Gudao High. The seven segments of arc EF correspond to the seven oil samples collected from the Gudao High. Each segment consists of two ribbons with different colours. The two ribbon widths linked to two EMs (arcs AB and CD) in one segment reflects the contribution percentages of EM1 and EM2. For example, >50% come from EM1, while less than 50% from EM2 in sample KG65 (Fig. 8a). In Fig. 8b, the length of the arc CD is five times longer than arc AB, which means that EM2 (Es_4^U) is the main source for the Luojia–Chenjiazhuang High. The 11 segments of arc EF correspond to the 11 oil samples collected from this area. Every ribbon connected to EM2 (arc AB) is much wider than that linked with EM1 (arc CD). For instance, the EM2 contribution is close to 100% in KX626. In Fig. 8c, arc CD is approximately three times as long as arc AB, suggesting that EM1

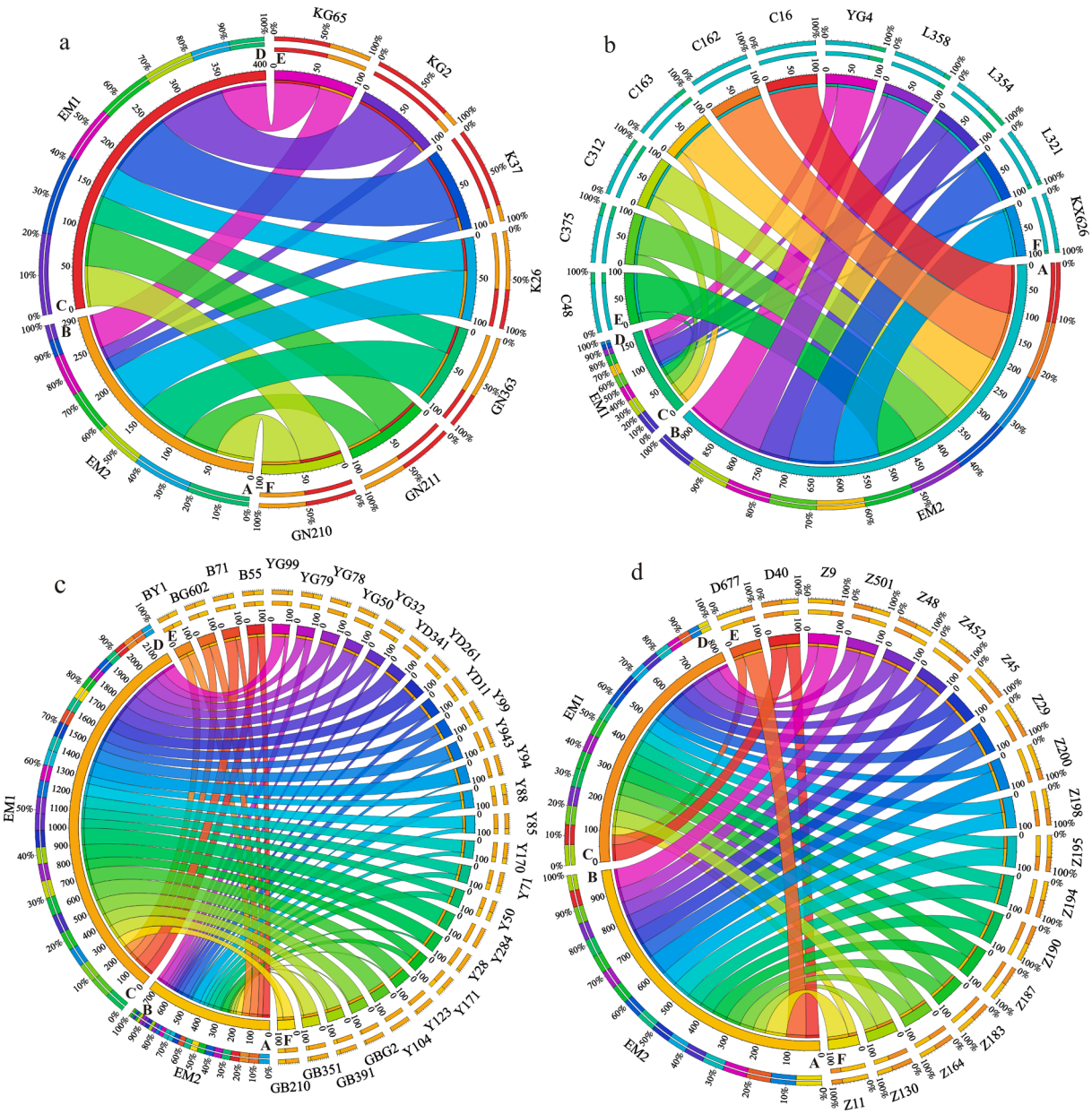

Fig. 8. Circos diagrams of the relative contributions of EM1 and EM2 to tectonic units and oils. (a) Gudao High, (b) Luojia–Chenjiazhuang High, (c) Bonan–Gubei Sag and (d) Yihezhuang Arch. Note: arc AB is proportional to the total contribution of EM2 to oils in a tectonic unit, arc CD is proportional to the total contribution of EM1. The segments on arc EF corresponds to the relative contribution of the two EMs for oil sample.

(Es_3^L) is the main source for the samples from the Bonan–Gubei Sag; it contributes more than three times as much as EM2 (Es_4^U). The 29 segments of arc EF correspond to the 29 oils collected from the Bonan–Gubei Sag. In Fig. 8d, the length of arc CD is slightly shorter than arc AB, which means that the contribution of EM2 (Es_4^U) is slightly higher than that of EM1 (Es_3^L) for samples from the Yihezhuang Arch. The 18 segments of arc EF correspond to the 18 oil samples collected from this area.

4.6. Maturity

In this work, several commonly aliphatic biomarker parameters based on the stability or transformation of molecules have been used to assess the oil maturity (Chen et al., 2011; Peters et al., 2005). The $C_{29}ααα20S/(20S + 20R)$, $C_{29}ββ/(αα + ββ)$, Ts/(Ts + Tm), and $diaC_{27}/regC_{27}$ ratios of oils from different areas significantly differ (Fig. 6).

Fig. 9 shows the isogram of $C_{29}ααα20S/(20S + 20R)$ steranes. It is notable that most oils from the Bonan–Gubei Sag have a higher maturity and oils from the Luojia–Chenjiazhuang High have low maturity. This might be related to the different fault activities during their sedimentation and different mineral compositions. During the deposition of the Es_4 member, block faulting activities were intensive; the basin was separated into many independent blocks (Jiu et al., 2013; Zhang et al., 2004). Therefore, the oil–gas migration channels well developed in both vertical and horizontal directions, providing extensive migration paths for hydrocarbons generated in the Es_4 member to other strata. The hydrocarbons migrated in the early mature stage. The Es_3 member was deposited in the differential subsidence of faulted depressions and the formation of deep lacustrine (Jiu et al., 2013; Zhang et al., 2004), the hydrocarbon could not migrate until another faulting activity occurred. The oils from the Es_3 member thus have higher maturity. During the early Es_4 deposition, grey mudstones with evaporite and gypsum were deposited, the source rock are often associated with formation waters with relatively high SO_4^{2-} concentrations (Shi et al., 2005). The overlying

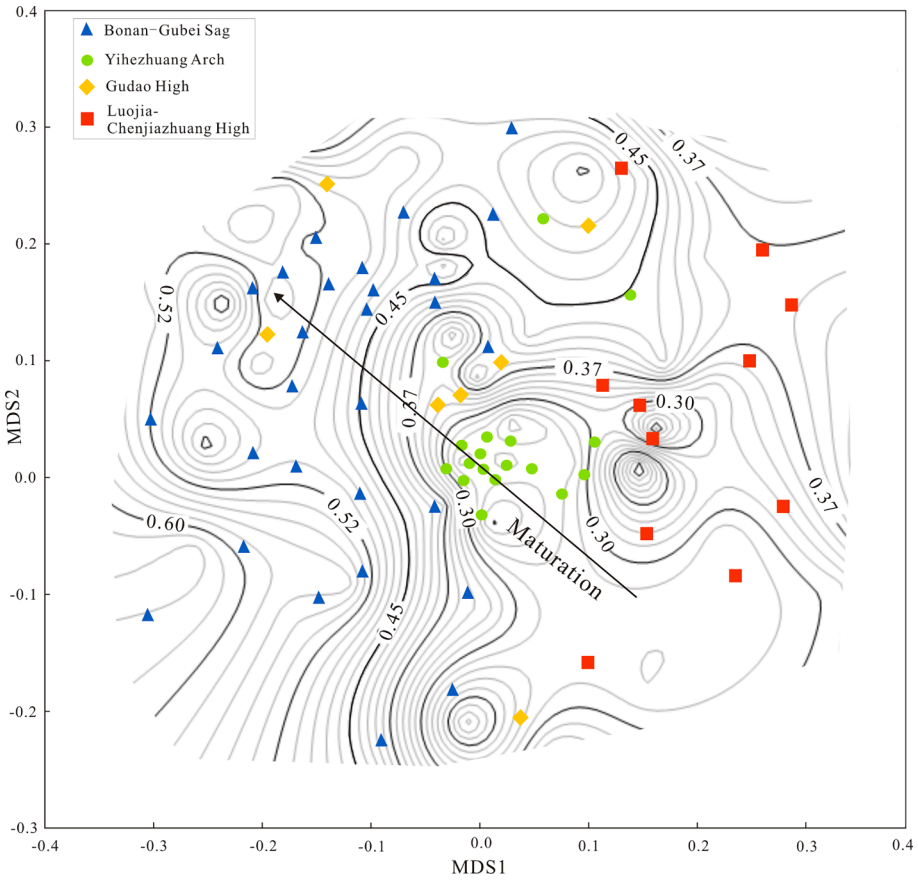

Fig. 9. MDS biplots showing the C_{29}ααα20S/(20S + 20R) isogram, arrows indicate expected trend with increased maturity.

Es_3 member is dominated by dark mudstone (Zhu et al., 2004). Gypsum–halite has negative effect on the biomarker maturity. With respect to C_{29} isomers (C_{29}Sαα and C_{29}Sββ, C_{29}Rαα and C_{29}Rββ), the transformation of the 20R and αα structures is retarded or inhibited compared with that of 20S and ββ in carbonates or evaporites (Chen et al., 2011). Therefore, the values of C_{29}ααα20S/(20S + 20R) and C_{29}ββ/(αα + ββ) steranes of oils from the Es_4^U shale are lower than those of oils from the Es_3^L shale. The maturity is related to the burial depth of the reservoir (Peters and Moldowan, 1993). Oils from the Bonan and Gubei sags in this study are mainly derived from the deep layer (~3000 m) and thus have a higher maturity. Oils from the Luojia–Chanjiazhang High and Yihezhuang Arch are mainly derived from the shallow layer (~1500 m) and therefore have relatively low maturity.

4.7. Variation of the mixing model in different tectonic units

The depositional centre of the Zhanhua Depression is marked by the Bonan–Gubei Sag (Zhang et al., 2007). Oils in this area were primarily derived from the source rocks deposited under freshwater–brackish lacustrine environments with a combination of microalgae material and terrigenous organic input. Based on the ALS, MDS, and circos, the Es_3^L shale is the main source rock in the depositional centre and contributes more than three times as much as the Es_4^U shale. For oil samples from the Luojia–Chenjiazhuang High, the Es_4^U shale is the main source rock, which was deposited in a saline reducing environment with microalgal/bacterial organic matter input. The contribution of the Es_4^U shale is slightly higher than the Es_3^L shale for the Yihezhuang Arch. The contribution of Es_3^L shale is slightly higher than the Es_4^U shale for the Gudao High.

The petroleum produced in the Bonan–Gubei Sag migrated to reservoirs after faulting activities occurred which provided good migration channels. The migration range of hydrocarbon originating from Es_4^U source rocks is larger than that of Es_3^L source rocks, especially in the longitudinal direction. The migration of hydrocarbon originating from Es_3^L source rocks dominates in the lateral direction.

5. Conclusions

The contributions of the Es_4^U and Es_3^L shale to crude oils collected from the Zhanhua Depression were determined using ALS and circos diagrams and the genetic relationships of the crude oils were distinguished using MDS.

The dominant contributor to oils from the Bonan Sag and Gubei Sag was the Es_3^L source rock. The major contributor to oils from the Luojia Nose and Chanjiazhang High is the Es_4^U source rock. The contribution of the Es_4^U shale is a slightly higher than that of the Es_3^L shale for oils originating from the Yihezhuang Arch. The contribution of Es_3^L shale to oils from the Gudao High is approximately twice that of the Es_4^U shale. The Es_3^L member is the primary source rock in the depositional centre, the contribution of the Es_4^U member increases with increasing distance from the depositional centre. The maturities of oils from different areas are significantly different due to the different fault activities, mineral compositions of sedimentary strata, and burial depths of the reservoirs.

In this study, we successfully deconvoluted the mixed oils collected in the Zhanhua Depression using ALS and identified the affinities of the crude oil samples using MDS. In addition, we introduced the circos diagram to clarify the relation between the EMs and different tectonic units and oils.

CRediT authorship contribution statement

Xiao–Hui Lin: Investigation, Writing - original draft. **Zhao–Wen**

Zhan: Formal analysis, Writing - review & editing. **Yan–Rong Zou:** Conceptualization, Methodology, Software. **Tian Liang:** Investigation, Writing - review & editing. **Ping'an Peng:** Supervision.

Declaration of Competing Interest

The authors declare that they have no known competing financial interests or personal relationships that could have appeared to influence the work reported in this paper.

Acknowledgements

We appreciate Prof. Liu Keyu and the two anonymous reviewers for their detailed and constructive comments that significantly improved the quality of the manuscript. We acknowledge Dr. Yao–Ping Wang for the kind help with this study. This study was funded by the Natural Science Funding Council of China (Grant No. 41621062), SKLOG project (SKLOGA 201701 SKLOGC 201704), and GIGCAS 135 project (Grant No. Y234021001).

References

Albaghdady, A.A., 2013. Organic Geochemical Characterization of Source Rocks (Sirt Shale) and Crude Oils from Central Sirt Basin, Libya (Ph.D. thesis). University of Oklahoma, Norman, 260.

Aquino Neto, F.R., Trendel, J.M., Restle, A., Connan, J., Albrecht, P.A., 1983. Occurrence and formation of tricyclic and tetracyclic terpanes in sediments and petroleum. Adv. Org. Geochem. 4, 659–667.

Blanc, P., Connan, J., 1992. Origin and occurrence of 25 norhopanes: a statistical study. Org. Geochem. 18, 813–828.

Cai, J., Dan, B., Zhang, C., 2005. Oil and source correlation of Sikou sag in Zhanhua Depression. P.G.O.D.D 24, 11–15 in Chinese with English abstract.

Chen, Z., Zha, M., Jin, Q., Ren, Y., 2011. Distribution of sterane maturity parameters in a lacustrine basin and their control factors: A case study from the Dongying Sag, East China. Pet. Sci. 8, 290–301.

Cheng, X., Mao, Z.C., Mao, R., Li, Z.Q., Guan, Q.S., Chen, X., 2018. Families of reservoired crude oils from Cangdong Sag, Bohai Bay Basin. China. Org. Geochem. 122, 115–125.

Dong, T., He, S., Liu, G., Hou, Y., Harris, N.B., 2015. Geochemistry and correlation of crude oils from reservoirs and source rocks in southern Biyang Sag, Nanxiang Basin. China. Org. Geochem. 80, 18–34.

Guo, Y.L., 2001. Distribution of proven petroleum reserves in the Jiyang Superdepression. Pet. Explor. Dev. 28, 33–35 in Chinese with English abstract.

Fang, X., 2017. Hydrocarbon migration paths and enrichment rules of Neogene in Zhanhua Sag of Bohai Bay Basin. Fault–block Oil and Gas Field 23, 300–304 in Chinese with English abstract.

Farrimond, P., Bevan, J.C., Bishop, A.N., 1996. Hopanoid hydrocarbon maturation by an igneous intrusion. Org. Geochem. 25, 149–164.

Hanson, A.D., 2000. Molecular Organic Geochemistry of the Tarim Basin, Northwest China. Am. Assoc. Pet. Geol. Bull. 84, 1109–1128.

Hao, F., Zhou, X., Zhu, Y., Zou, H., Bao, X., Kong, Q., 2009. Mechanisms of petroleum accumulation in the Bozhong sub–basin, Bohai Bay Basin, China. Part 1: Origin and occurrence of crude oils. Mar. Pet. Geol. 27, 1528–1542.

Hao, F., Zhou, X., Zhu, Y., Zou, H., Yang, Y., 2010. Charging of oil fields surrounding the Shaleitian uplift from multiple source rock intervals and generative kitchens, Bohai Bay basin. China. Mar. Pet. Geol. 27, 1910–1927.

Harris, N.B., Freeman, K.H., Pancost, R.D., White, T.S., Mitchell, G.D., 2004. The character and origin of lacustrine source rocks in the Lower Cretaceous synrift section, Congo Basin, west Africa. Am. Assoc. Pet. Geol. Bull. 88, 1163–1184.

Holba, A.G., Dzou, L.I., Wood, G.D., Ellisd, L., Adam, P., Schaeffer, P., Albrecht, P., Greene, T., Hughes, W.B., 2003. Application of tetracyclic polyprenoids as indicators of input from fresh–brackish water environments. Org. Geochem. 34, 441–469.

Huang, L., Liu, C., 2014. Evolutionary characteristics of the sags to the east of Tan–Lu Fault Zone, Bohai Bay Basin (China). Implications for hydrocarbon exploration and regional tectonic evolution. J. Asian Earth Sci. 79, 275–287.

Hunt, J., 1996. Petroleum Geochemistry and Geology. W. H. Freeman and Company, USA, p. 743.

Jiu, K., Ding, W., Huang, W., Zhang, Y., Zhao, S., Hu, L., 2013. Fractures of lacustrine shale reservoirs, the Zhanhua Depression in the Bohai Bay Basin, eastern China. Mar. Pet. Geol. 48, 113–123.

Li, S., Pang, X., Jin, Z., 2004. Application of biomarkers to quantitative source assessment of oil pool. Acta Geol. Sin. 78, 784–790.

Li, S., Pang, X., Jin, Z., Li, M., Liu, K., Jiang, Z., Qiu, G., Gao, Y., 2010. Molecular and isotopic evidence for mixed–source oils in subtle petroleum traps of the Dongying South Slope, Bohai Bay Basin. Mar. Pet. Geol. 27, 1411–1423.

Lin, H., Fang, Q., Li, L., Lin, Y., Li, H., Li, W., Wu, Z., 2007. Development of bur ied hills of the eastern Zhanhua subbasin, Jiyang depression, northern Shandong, China and controlling factors of the formation of petroleum accumulations. Geol. Bull. China. 25, 1170–1177 in Chinese with English abstract.

Lin, X., 2021. Petroleum geochemometrics differentiation of crude oils-Case studies on oils in the central of the Jiyang Depression. University of Chinese Academy of Sciences.

Lu, H., Jiang, Y., Liu, H., Zhang, H., Liu, Y., 2012. Study on formation stages of oil–gas reservoirs in Bonan Subsag. Zhanhua Sag. Pet. Geol. Recovery Effic. 19, 5–8 in Chinese with English abstract.

Martin, H., Nishadi, D.S., Thomas, D.O., Julian, P., Jacqueline, A.K., Simon, R.H., 2015. Circlator: Automated circularization of genome assemblies using long sequencing reads. Genome Biol. 16, 1–17.

Martin, K., Jacqueline, S., Inanc, B., Joseph, C., Randy, G., Doug, H., Steven, J.J., Marco, A.M., 2009. Circos: An information aesthetic for comparative genomics. Genome Res. 19, 1739–1745.

Moldowan, J.M., Fago, F.J., Carlson, R.M.K., Young, D.C., an Duvne, G., Clardy, J., Schoell, M., Pillinger, C.T., Watt, D.S., 1991. Rearranged hopanes in sediments and petroleum. Geochim. Cosmochim. Acta. 55, 3333–3353.

Peters, K.E., Hostettler, F.D., Lorenson, T.D., Rosenbauer, R.J., 2008a. Families of Miocene Monterey crude oil, seep, and tarball samples, coastal California. Am. Assoc. Pet. Geol. Bull. 92, 1131–1152.

Peters, K.E., Moldowan, J.M., 1991. Effects of source, thermal maturity, and biodegradation on the distribution and isomerization of homohopanes in petroleum. Org. Geochem. 17, 47–61.

Peters, K.E., Moldowan, J.M., 1993. The Biomarker Guide. Interpreting Molecular Fossils in Petroleum and Ancient Sediments. Prentice Hall, Englewood Cliffs, New Jersey.

Peters, K.E., Moldowan, M.J., Mccaffrey, M.A., Fago, F.J., 1997. Selective biodegradation of extended hopanes to 25–norhopanes in petroleum reservoirs: Insights from molecular mechanics. Org. Geochem. 24, 775–783.

Peters, K.E., Scott Ramos, L., Zumberge, J.E., Valin, Z.C., Bird, K.J., 2008b. De–convoluting mixed crude oil in Prudhoe Bay Field, North Slope. Alaska. Org. Geochem. 39, 723–745.

Peters, K.E., Scott Ramos, L., Zumberge, J.E., Valin, Z.C., Scotese, C.R., Gautier, D.L., 2007. Circum-Arctic petroleum systems identified using decision–tree chemometrics. Am. Assoc. Pet. Geol. Bull. 91, 877–913.

Peters, K.E., Walters, C.C., Moldowan, J.M., 2005. The Biomarker Guide. Cambridge University Press, Cambridge, UK.

Shi, D., Li, M., Pang, X., Chen, D., Zhang, S., Wang, Y., Jin, Q., 2005. Fault–fracture mesh petroleum plays in the Zhanhua Depression, Bohai Bay Basin: Part 2. Oil–source correlation and secondary migration mechanisms. Org. Geochem. 37, 203–223.

Sinninghe Damsté, J.S., Kenig, F., Koopmans, M.P., Koster, J., Schouten, S., Hayers, J.M., de Leeuw, J.W., 1995. Evidence for gammacerane as an indicator of water column stratification. Geochim. Cosmochim. Acta. 59, 1895–1900.

Summons, R.E., Hope, J.M., Swart, R., Walter, M.R., 2008. Origin of Nama Basin bitumen seeps: petroleum derived from a Permian lacustrine source rocks traversing southwestern Gondwana. Org. Geochem. 11, 589–607.

Sun, Y., Sheng, G., Peng, P.A., Fu, J., 2000. Compound–specific stable carbon isotope analysis as a tool for correlating coal–sourced oils and interbedded shale–sourced oils in coal measures: An example from Turpab basin, north–western China. Org. Geochem. 31, 1349–1372.

Sun, Y.T., Xu, S.Y., Zhang, S.Q., Liu, J.H., Gong, J.Q., Meng, T., Li, H., 2015. Reservoir characteristics and reservoir–forming model of multi–element hydrocarbon supply in Zhanhua Sag. J. China Univ. Pet. 39, 42–49 in Chinese with English abstract.

Volkman, J.K., 1986. A review of sterol markers for marine and terrigenous organic matter. Org. Geochem. 9, 83–99.

Wang, H., Hu, Y., 2014. Analysis of influence factors of shale oil formation in Zhanhua Depression of Bohai Bay Basin. Nat. Gas Geosci. 25, 141–149 in Chinese with English abstract.

Wang, Y.-P., Zhang, F., Zou, Y.-R., Sun, J.-N., Lin, X.-H., Liang, T., 2018. Oil source and charge in the Wuerxun Depression, Hailar Basin, northeast China: A chemometric study. Mar. Pet. Geol. 89, 775–787.

Wang, Y.-P., Zhang, F., Zou, Y.-R., Zhan, Z.-W., Peng, P.A., 2016. Chemometrics reveals oil sources in the Fangzheng Fault Depression, NE China. Org. Geochem. 102, 1–13.

Wang, Y., Li, M., Pang, X., Zhang, S., Shi, D., 2005. Fault–fracture mesh petroleum plays in the Zhanhua Depression, Bohai Bay Basin: Part 1. Source rock characterization and quantitative assessment. Org. Geochem. 37, 183–202.

Wang, Y., Liu, H., Song, G., Jiang, X., Zhu, D., Yang, W., 2017. Enrichment controls and models of shale oil in the Jiyang Depression, Bohai Bay Basin. J. China Univ. Geol. 23, 278–1277 in Chinese with English abstract.

Wang, Y., Song, G., Liu, H., Jiang, X., Hao, X., Ning, F., 2015. Main control factors of enrichment characteristics of shale oil in Jiyang depression. Pet. Geol. Recovery Effic. 22, 20–25 in Chinese with English abstract.

Xie, Q.L., Liu, Z., 2006. Study on the conditions and characteristics of hydrocarbon migration in the south slope of Zhanhua Sag. Xinjiang oils and gas. 2, 11–15 in Chinese with English abstract.

Yu, Y., Zhou, X., Xu, C., Wu, K., Lv, D., Liu, Y., Zhou, X., 2020. Architecture and evolution of the Cenozoic offshore Bohai Bay Basin, eastern China. J. Asian Earth Sci. 192.

Zhan, Z.W., Tian, Y., Zou, Y.-R., Liao, Z., Peng, P.A., 2016a. De–convoluting crude oil mixtures from Palaeozoic reservoirs in the Tabei Uplift, Tarim Basin. China. Org. Geochem. 97, 78–94.

Zhan, Z.W., Zou, Y.-R., Shi, J.-T., Sun, J.-N., Peng, P.A., 2016b. Unmixing of mixed oil using chemometrics. Org. Geochem. 92, 1–15.

Zhan, Z.W., Lin, X.H., Zou, Y.R., Li, Z., Wang, D.Y., Liu, C., Peng, P.A., 2019. Chemometric differentiation of crude oil families in the southern Dongying Depression, Bohai Bay Basin. China. Org. Geochem. 127, 37–49.

Zhang, L., Xu, X., Liu, Q., Kong, X., Zhang, S., 2011. Hydrocarbon formation and accumulation of the deep Paleogene of the Jiyang Depression, Shengli Oilfield. Pet. Explor. Dev. 38, 530–537.

Zhang, L., Liu, Q., Zhu, R., Li, Z., Lu, X., 2009. Source rocks in Mesozoic-Cenozoic continental rift basins, East China: a case from Dongying Depression, Bohai Bay Basin. Org. Geochem. 40, 229–242.
Zhang, L.Y., Lin, Q., Xu, X.Y., Li, J.Y., Zhang, S.C., 2015. Oil and gas geochemistry and fine exploration of mature petroleum exploration area. Petroleum Industry Press, Beijing, p. 199 in Chinese.
Zhang, S.W., Wang, Y.S., Shi, D.S., Xu, H.M., Pang, X., Li, M., 2004. Fault–fracture mesh petroleum plays in the Jiyang Superdepression of the Bohai Bay Basin, eastern China. Mar. Pet. Geol. 21, 751–778.
Zhang, S., Zhang, L., Li, Z., Hao, Y., 2012. Formation conditions of Paleogene shale oil and gas in Jiyang Depression. Pet. Geol. Recovery Effic. 19, 1–5 in Chinese with English abstract.
Zhang, Z., Zeng, Y., Zhang, X., Yuan, D., Xu, X., 2007. The geochemistry characteristics and accumulation history of crude oil in the Bonan sub sag of the Zhanhua sag, the Bihaiwan basin. Pet. Geol. Exp. 28, 54–59 in Chinese with English abstract.
Zhao, W.Z., Chi, Y.L., 2000. Occurrence and origins of major petroleum accumulation zones in the Bohai Bay Basin. Pet. Acta 21, 10–15 in Chinese with English abstract.
Zhu, G., Jin, Q., Zhang, S., Dai, J., Zhang, L., Li, J., 2004. Distribution characteristics of effective source rocks and their control on hydrocarbon accumulation: A case study from the Dongying Sag. Eastern China. Acta Geol. Sin. 78, 1275–1288.
Zytkow, J.M., Rauch, J., 1999. Principles of data mining and knowledge discovery. In: Third European Conference on Principles and Practice of Knowledge Discovery in Databases, PKDD'99, pp. 277–282.

Further reading

Chen, J., Deng, C., Song, F., Zhang, D., 2007. Mathematical calculating model using biomarkers to quantitatively determine relative source proportion of mixed oils. Geochimica 36, 205–214 in Chinese with English abstract.
Collister, J.W., Wavrek, D.A., 1996. δ13C compositions of saturate and aromatic fractions of lacustrine oils and bitumens: evidence for water column stratification. Org. Geochem. 24, 913–920.
Isaksen, G.H., Bohacs, K.M., 1995. Geological controls of source rock geochemistry through relative sea level; Triassic. Barents Sea. Pet. Source Rocks. 25–50.
Pancost, R.D., Freeman, K.H., Patzkowsky, M.E., Wavrek, D.A., Collister, J.W., 1998. Molecular indicators of redox and marine photoautotroph composition in the late Middle Ordovician of Iowa, U.S.A. Org. Geochem 29, 1649–1662.
Philp, R.P., Gilbert, T.D., 1987. Biomarker distributions in Australian oils predominantly derived from terrigenous source material. Org. Geochem. 10, 73–84.
Sofer, J., 1984. Stable carbon isotope compositions of crude oils: Application to source depositional environments and petroleum alteration. Am. Assoc. Pet. Geol. Bull. 68, 31–49.
Xue, Y., Yu, H., Xiang, H., 2007. A comparative study on hydrocarbon enrichment of main sags in Bohai Bay basin. China Offshore Oil and Gas 19, 145–149 in Chinese with English abstract.